Thermodynamic Calculations in the Modeling of Multiphase Processes and Reactors

Anna Yermakova* and Vladimir I. Anikeev

Boreskov Institute of Catalysis, Pr. Lavrentieva, 5, Novosibirsk 630090, Russia

A two-parameter cubic Soave−Redlich−Kwong (SRK) equation of state with modified binary interaction coefficients has been used for phase equilibrium calculations of multicomponent systems under supercritical and near-supercritical conditions. Example calculations of the phase behavior of multicomponent reaction mixtures are presented and used to illustrate the increased accuracy of the SRK equation of state with the new binary interaction coefficients. The homotopy continuation method was adapted for the solution of the model equations by using temperature and pressure as continuation parameters. The effective models and algorithms thus created are used for phase state calculations, localization of the critical point of multicomponent mixtures, studies of phase properties near the critical point, and determination of parameter regions that are of practical importance for process performance under supercritical conditions. The problems of existence and uniqueness of a solution are studied. A new method for solving equations for the critical phase is suggested. Many examples of the calculation of phase diagrams of mixtures with a supercritical solvent are presented and the results compared with the reference data. Thermodynamic and macrokinetic models of the Fischer−Tropsch (FT) reaction are developed and used for the calculation of reactor performance.

Contents

1. Introduction

Three-phase catalytic reactors have been used extensively in many chemical, petrochemical, and biochemical process engineering applications. Liquid-phase oxida-

* To whom correspondence should be addressed. Fax: 7 383 23974 47. E-mail: anna@catalysis.nsk.su.

10.1021/ie9905761 CCC: $19.00
Published on Web 04/13/2000

tion, hydrogenation, alkylation, and so forth are a few among these processes. Such multiphase reactors (slurry bubble column) have a significant application in the Fischer−Tropsch synthesis of syn gases on a suspended catalyst.

Many monographs describing the various aspects of multiphase reactors (heat- and mass-transfer characteristics, hydrodynamic behavior, and slurry mixing) appeared in recent years. The development and optimization of multiphase processes requires the knowledge of the phase behavior, the amount and composition of phases, the solubility of the components, and enthalpy of phase conversions at the reaction conditions subject to nonideality of reaction mixtures. In this connection the thermodynamic calculations are necessary for mathematical modeling. Along with the experimental methods, mathematical modeling is of great help in obtaining knowledge about processes. Moreover, mathematical modeling is preferred in some cases because experimental studies of multiphase multicomponent chemical reactions are very complicated.

To model the phase states of multicomponent reaction mixtures, thermodynamic models providing realistic descriptions of $P-V-T$ properties over a wide range of temperatures and pressures have been actively used in recent years.

A large family of thermodynamic models, suggested for calculations of phase equilibrium, uses cubic equations of state which include the binary interaction coefficients. These equations make a nice instrument for calculations of thermodynamic properties and phase equilibrium of multicomponent nonideal mixtures.

Thermodynamic models are especially important for the study and modeling of multiphase processes occurring at or near supercritical states of the reaction mixture.

Such processes usually proceed in the high-pressure and -temperature region, either in the presence of some inert supercritical solvent or during the time when one of the reaction products acts as a supercritical solvent. Peculiar properties of the "supercritical medium" (low viscosity, high mutual solubility of components, high diffusion, etc.) are usually exhibited in the region ranging from the critical temperature and pressure of the supercritical solvent to those of the reaction mixture. Because of its extraordinary properties, this region (hereafter named as the "supercritical" region) is very promising for the performance of homogeneous and heterogeneous catalysis. One can control the reactions by choosing a solvent and its concentration.

In the supercritical region (except the mixture critical point), the two-phase state still holds. However, this state is not stable and is extremely sensitive to changes in the mixture composition, temperature, and pressure that may occur in the course of the chemical reaction. Densities of fluid phases in this region are comparable and range from the density of gas to that of liquid. More, the solvent concentration in both phases is approximately similar.

The high sensitivity of the medium properties to changes in parameters, and the probable appearance or disappearance of phases in the course of the chemical reaction, indicate that thermodynamic calculations should play a more important role in the mathematical modeling of multiphase processes, especially under near-to-critical conditions. Therefore, software and algorithms for calculations of phase behavior of complex mixtures, performed on the basis of rigorous thermodynamic models, must be included in programs simulating the operation of reactors and technologies.

In the present paper, we discuss the typical phase behavior of multicomponent reaction mixtures and problems associated with calculations of multicomponent reactors operating under phase-transition conditions. The goal is to develop simple methods and robust algorithms for calculations of phase states (yield and composition and thermodynamic stability of equilibrium phases) in complex mixtures as a part of the multiphase reactor model software. Of special interest are the problems related to the localization of the critical point of multicomponent mixtures, studies of phase properties near the critical point, and determination of parameter (temperature and pressure) regions that are of practical importance for process performance under supercritical conditions. The use of thermodynamic models for calculations of reactor performance are exemplified. The models discussed in this article are based on the theoretical fundamentals of multiphase thermodynamics.

For a steady-state or quasi-steady-state equilibrium process, the thermodynamic model reduces to a system of nonlinear algebraic equations, whose parameters are usually temperature and pressure in applied problems. These parameters can be measured and controlled during experimental tests of the model. The steady-state model of the perfectly mixed reactor also reduces to a system of nonlinear equations with parameters. The well-known homotopy continuation method is adapted for the solution of model equations by using the temperature and pressure as continuation parameters. The created effective algorithms are part of the reactor and the flow sheet modeling program package.

Because the kinetic model of a chemical reaction is an obligatory element of the reactor mathematical model, we have considered the problems related to construction of the "global" kinetic model. On one hand, this model should show the detailed mechanism of the reaction. On the other hand, one needs "global" experimental kinetic data to determine the model parameters, which permits one to express reaction rates in the same terms of extensive and intensive values used in the reactor mathematical model. In a complex multicomponent reaction system, the concentration data measured in the kinetic experiments are not always sufficiently sensitive to develop a detailed reaction mechanism. Therefore, the global kinetic data allow the use of some phenomenological elements, provided the model is consistent with the experimental data. Upon development of a macrokinetic model of some complex reaction, one uses statistical methods for data reconciliation, providing the information on the experimental data quality and algorithms for the calculation of model parameters and analysis of their reliability. The methodology used is briefly described in this paper. The software for statistic processing of the experimental data is also a part of the general software for reactor calculations.

2. Base Model for the Description of $P-V-T$ Properties of Multicomponent Mixtures

Phase equilibrium is usually calculated by three-parameter cubic equations of state (EOS) such as Soave−Redlich−Kwong, Peng−Robinson, Patel−Teja, and so forth.[1] In most cases, these EOSs nicely describe

the $P-V-T$ properties of all fluid phases. Therefore, the undoubted advantage will be the modeling of a multiphase system using a unified model EOS for all fluid phases.

2.1. Modified Soave−Redlich−Kwong Equation of State. The Soave−Redlich−Kwong (SRK) equation of state for multicomponent mixtures is[2]

$$P = \frac{RT}{v_m - b_m} - \frac{a_m(T)}{v_m(v_m + b_m)} \quad (1)$$

$$a_m = \sum_{j=1}^{N}\sum_{i=1}^{N} x_i x_j a_{ij} \quad (2)$$

$$b_m = \sum_{j=1}^{N}\sum_{i=1}^{N} x_i x_j b_{ij} \quad (3)$$

$$a_{ii} = \alpha_i(T)(0.42748R^2 T_{ci}^{\ 2}/P_{ci}) \quad (4)$$

$$b_{ii} = 0.08664RT_{ci}/P_{ci} \quad (5)$$

$$a_{ij} = (1 - k_{ij})\sqrt{a_{ii}a_{jj}} \quad (6)$$

$$b_{ij} = (1 - c_{ij})(b_{ii} + b_{jj})/2 \quad (7)$$

$$\alpha_i(T) = [1 + m_i(1 - \sqrt{T/T_{ci}})]^2 \quad (8)$$

$$m_i = 0.480 + 1.574\omega_i - 0.176\omega_i^{\ 2} \quad (9)$$

where T_{ci},P_{ci}, and ω_i are the critical temperature, pressure, and the acentric factor of the ith component, x_i and x_j are the molar fractions of mixture components, $V_m = V_m(a_m,b_m,T,P)$ is the molar volume of the mixture, and k_{ij} and c_{ij} are the empirical mixing parameters.

The fugacity is expressed from equation of state (1):[1]

$$\ln f_i = \ln[x_i RT/(v_m - b_m)] + \beta_i/(v_m - b_m) + \frac{\gamma_i\beta_i}{RTb_m^{\ 2}}\left[\ln\left(\frac{v_m + b_m}{v_m}\right) - \frac{b_m}{(v_m + b_m)}\right] - \frac{\gamma_i}{RTb_m}\ln\left(\frac{v_m + b_m}{v_m}\right) \quad (10)$$

where

$$\gamma_i = 2\sum_{j=1}^{N_c} x_j a_{ij}, \qquad \beta_i = 2\sum_{j=1}^{N_c} x_j b_{ij} - b_m \quad (11)$$

The fugacity coefficient Φ_i and chemical potential μ_i are determined as

$$\Phi_i = f_i/Px_i; \qquad \mu_i = RT\ln f_i \quad (12)$$

Molar volumes of phases in eq 10 are calculated as polynomial roots:

$$Z^3 - Z^2 - Z(B^2 - B + A) - AB = 0 \quad (13)$$

where

$$Z = PV_m/RT, \qquad A = a_m P^2/(RT)^2, \qquad B = b_m P/RT \quad (14)$$

One chooses an arbitrary equation of state for calculations of system phase equilibrium. But the chosen equation should be universal and applicable for description of all fluid phases, when operational conditions and mixture composition vary over a wide range.

From the above reasoning, we decided to tune eq 1 using the empirical coefficients k_{ij} and c_{ij} which allow for binary interaction between the ith and jth components ($i = 1, 2, ..., N_c$, $i \neq j$).

2.2. Determination of the Binary Interaction Coefficients Using Experimental Data. Coefficients k_{ij} and c_{ij} are determined from the experimental data on the equilibrium in two-phase systems. In our examples, we referred to ref 3 which systematizes the experimental data on the vapor−liquid and gas−liquid equilibrium over a wide range of temperatures and pressures, including the region of critical conditions.

The constants were calculated by minimization of the functional as

$$S = \sum_{k=1}^{K}\left[\sum_{i=1}^{2}\left(\frac{\tilde{x}_{ik} - \bar{x}_{ik}}{\sigma_{xi}}\right)^2 + \sum_{i=1}^{2}\left(\frac{\tilde{y}_{ik} - \bar{y}_{ik}}{\sigma_{yi}}\right)^2\right] \rightarrow \min \quad (15)$$

Subject to the constraints was the equality of the component fugacity in the vapor-gas and liquid phases:

$$F_{ik} \equiv f_{ik}^{L}(\bar{x}_{1k},x_{2k},T,P,k_{12},c_{12}) - f_{ik}^{G}(\bar{y}_{1k},\bar{y}_{2k},T,P,k_{12},c_{12}) = 0, \quad i = 1, 2; \quad k = 1, 2, ..., K \quad (16)$$

The following conditions were also taken into account as restrictions:

$$\sum_{i=1}^{2}\bar{x}_{ik} = 1, \qquad \sum_{i=1}^{2}\bar{y}_{ik} = 1 \qquad k = 1, 2, ... K \quad (17)$$

In eqs 15−17, indices k and i denote the number of the experimental point and component, respectively. The experimental molar fractions of components in the liquid and vapor-gas phases are denoted as $\tilde{x}_{ik}$ and $\tilde{y}_{ik}$, respectively, whereas $\bar{x}_{ik}$ and $\bar{y}_{ik}$ are their adjusted values, which minimize function (15) and satisfy eqs 16 and 17. The relative errors σ_{xi} and σ_{yi} are usually $0.05\tilde{x}_{ik}$ and $0.05\tilde{y}_{ik}$, respectively. f_{ik}^{L} and f_{ik}^{G} are the fugacity of the ith component in the liquid and gas phases in a kth run.

The effective numerical algorithms for the solution of the minimization problems (15)−(17) are described elsewhere.[4,5] The estimated parameters k_{ij} and c_{ij} fit the polynomial dependences $T_{r2} = T/T_{c2}$ and $P_{r2} = P/P_{c2}$, where T_{c2} and P_{c2} are the critical temperature and pressure of the heavier component in the binary mixture. Polynomial dependencies providing good approximations of k_{ij} and c_{ij} for all pairs studied are

$$k_{12} = k_{21} = \sum_{q=0}^{1}\sum_{p=0}^{2} A_{pq} T_{r2}^{p} P_{r2}^{q} \quad (18)$$

$$c_{12} = c_{21} = \sum_{q=0}^{1}\sum_{p=0}^{2} B_{pq} T_{r2}^{p} P_{r2}^{q} \quad (19)$$

Equations 18 and 19 are for T_{r2} ranging from 0.3 to 0.97. Tables 1 and 2 illustrate the derived values of the coefficients in eqs 18 and 19 for a number of binary pairs.

Table 1. Coefficients in Eq 18

binary pair	A_{00}	A_{01}	A_{02}	A_{10}	A_{11}	A_{12}	intervals of P_{r2}
$H_2-C_3H_8$	−2.932	6.448	−3.266	−0.5055	1.456	−1.044	1−14
$H_2-C_6H_6$	−0.9124	3.457	−2.935	−0.03036	0.1022	−0.09266	5−60
H_2-NH_3	1.057	0.5694	−1.750	−1.685	3.750	−2.077	0.5−4
N_2-NH_3	−7.794	21.610	−14.24	1.880	−4.790	2.957	0.5−4
$N_2-C_6H_6$	0.4329	−0.7749	0.0	0.0	0.0	0.0	1−6
$N_2-C_{10}H_{22}$	−3.075	6.727	−1.516	0.3184	−0.8094	0.3796	2.5−16
$CO-C_3H_8$	−0.2061	0.4183	0.0	0.1104	−0.2078	0.0	2−4.5
$CH_4-C_3H_8$	0.09241	−2.150	4.484	−0.1205	1.676	−3.068	0.5−2.5
$CH_4-C_{10}H_{22}$	−1.522	4.841	−3.554	0.1429	−0.4334	0.3055	0.2−16
$C_4H_{10}-C_{10}H_{22}$	−0.1427	0.5172	−0.3941	−1.819	4.565	−2.845	0.5−4

Table 2. Coefficients in Eq 19

binary pair	B_{00}	B_{01}	B_{02}	B_{10}	B_{11}	B_{12}	intervals of P_{r2}
$H_2-C_3H_8$	−0.8063	2.069	−1.462	−0.1681	0.4666	−0.3162	1−14
$H_2-C_6H_6$	−0.1014	0.3966	−0.4669	−0.01238	−0.03398	0.02428	5−60
H_2-NH_3	−0.05320	1.262	−1.550	−0.5495	1.2170	−0.6313	0.5−4
N_2-NH_3	−5.936	15.76	−10.35	2.002	−5.108	3.224	0.5−4
$N_2-C_6H_6$	0.07557	−0.2257	0.0	0.0	0.0	0.0	1−6
$N_2-C_{10}H_{22}$	−1.520	4.527	−3.128	0.1202	−0.3619	0.2484	2.5−16
$CO-C_3H_8$	0.1190	−0.1008	0.0	0.04752	−0.1182	0.0	2−4.5
$CH_4-C_3H_8$	−0.1586	−0.7920	2.540	−0.0037	0.7994	−1.776	0.5−2.5
$CH_4-C_{10}H_{22}$	−1.082	3.480	−2.626	0.0703	−0.2128	0.1375	0.2−16
$C_4H_{10}-C_{10}H_{22}$	−0.7484	2.150	−1.502	−2.647	6.859	−4.399	0.5−4

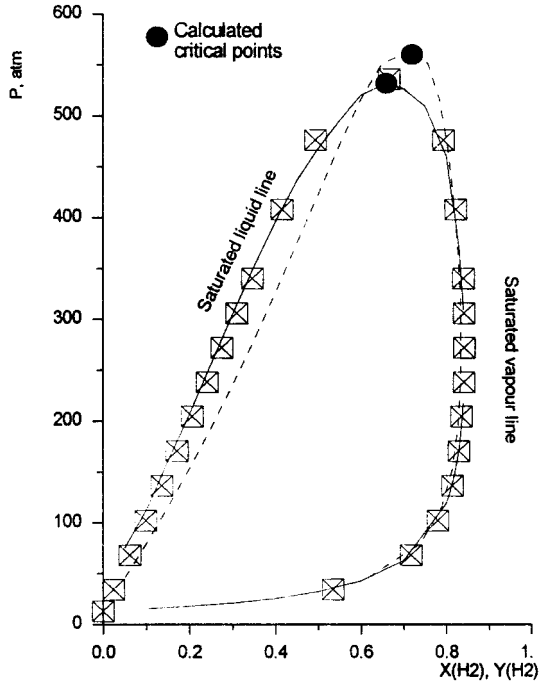

Figure 1. Phase diagram "pressure−composition" for the binary mixture $H_2-C_3H_8$ at $T = 310.8$ K. Solid lines stand for calculation via the SRK model allowing for k_{ij} and c_{ij}; dotted lines stand for $k_{ij} = 0$, $c_{ij} = 0$. Squares denote experimental data.[3]

2.3. Examples and Comparative Analysis. Figures 1 and 2 exemplify an increase in the accuracy of the SRK EOS when one uses the above corrections. The phase diagram "pressure−composition" is built for the system $H_2-C_3H_8$ at $T_{r2} = 0.39$ (310.8 K). Solid lines denote calculated curves with allowance for coefficients k_{12} and c_{12}, and broken lines indicate calculations at $k_{12} = 0$ and $c_{12} = 0$. Dots correspond to the experimental data.[3]

As shown in Figure 1, the saturated vapor line is practically insensitive to correction terms until a certain pressure value is reached. Note that this value is rather distant from the critical point. The saturated liquid line calculated without corrections differs significantly from the experimental data. This data deviation is observed near the critical pressure. In addition, the coordinates of the critical point with allowance for coefficients k_{12} and c_{12} are reproduced with high accuracy.

In Figure 2a,b, the SRK model is used to describe the solubility of liquid components in the compressed gases. This situation is usually observed when chemical reactions are performed at high pressures. Anomalous behaviors of some gas solutions, such as benzene in compressed nitrogen, and extreme points on the curve of solubility versus pressure have engaged the attention of researchers.[6] It is evident that these anomalies cannot be described by the Raoult−Henry equations. Calculations were performed with and without allowances for k_{12} and c_{12}. Note that correction terms for the binary system $N_2-C_6H_6$ at 348 and 373 K were obtained using experimental data.[3] A comparison was performed using the data of ref 3 and "independent" data of Krichevskii.[6] The latter data go far beyond the pressure limits where k_{12} and c_{12} were determined. According to Figure 2a,b the model extrapolated to the region of high pressures describes with high accuracy the experimental data of Krichevskii.[6] But the possibility of the extrapolation must not be generalized and should be checked experimentally in each particular case.

One may conclude that the empirical parameters k_{ij} and c_{ij} and their dependence on temperature and pressure permit one to describe accurately thermodynamic properties of mixtures in the region of high pressure and temperature and near the critical points.

3. Method for Phase Diagrams Calculations

One of the steps of thermodynamic calculations of a multiphase reactor is the determination of the regions where the mixture with a given composition is thermodynamically stable and homogeneous and the regions where the mixture is unstable and splits into two or several phases.[7] To solve this problem, it necessary to construct the two- or multiphase boundaries on various types of diagrams (pressure−temperature, pressure−composition, and temperature−composition). Critical points on the multiphase boundaries are also estimated during diagram construction.

3.1. Mathematical Model for a Two-Phase Equilibrium. Let us consider first the well-known phase-

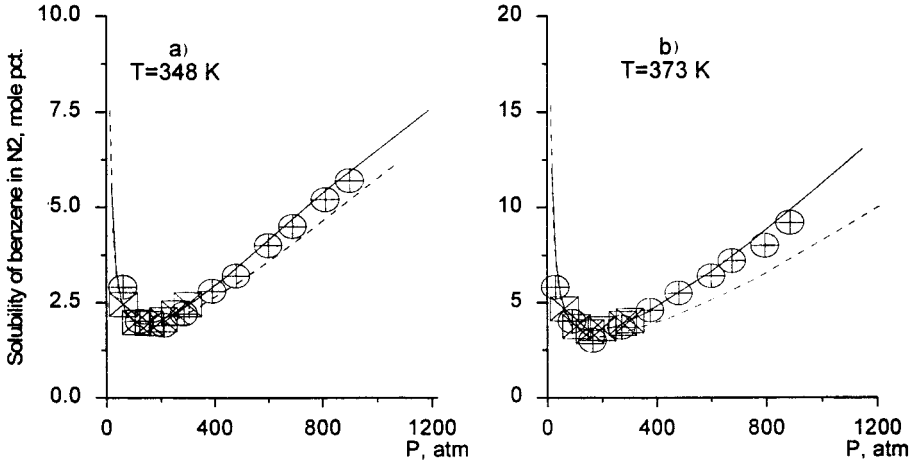

Figure 2. (a,b) Solubility of benzene in compressed nitrogen as a function of pressure. Solid lines denote calculations using the SRK model with allowance for k_{ij} and c_{ij}; dotted lines stand for $k_{ij} = 0$, $c_{ij} = 0$. Points are the experimental data.[3,6]

split problem.[8] Starting with a single phase of total mole number, $L^{(0)}$, component mole numbers, $n_i^{(0)}$, and mole fractions, z_i ($i = 1, 2, ..., N$). It is suggested that this mixture divides into two phases. Let $n_i^{(1)}$ and $n_i^{(2)}$ ($i = 1, 2, ..., N$) stand for mole numbers of these phases. The yield of phases, phase concentrations, and balance constraints between variables under conditions of material isolation are determined as

$$L^{(1)} = \sum_{i=1}^{N} n_i^{(1)}, \qquad L^{(2)} = \sum_{i=1}^{N} n_i^{(2)}, \qquad L^{(0)} = L^{(1)} + L^{(2)} \tag{20}$$

$$x_i = \frac{n_i^{(1)}}{L^{(1)}}, \qquad y_i = \frac{n_i^{(2)}}{L^{(2)}}, \qquad z_i = \frac{n_i^{(0)}}{L^{(0)}} \tag{21}$$

$$W_x = L^{(1)}/L^{(0)}, \qquad W_y = L^{(2)}/L^{(0)}, \qquad W_x + W_y = 1 \tag{22}$$

$$W_x x_i + W_y y_i = z_i, \qquad i = 1, 2, ..., N \tag{23}$$

$$y_i = z_i/(1 + W_x(K_i - 1)), \qquad x_i = K_i z_i/(1 + W_x(K_i - 1)) \tag{24}$$

$$\varphi \equiv \sum_{i=1}^{N} (x_i - y_i) = \sum_{i=1}^{N} \frac{z_i(K_i - 1)}{1 + W_x(K_i - 1)} = 0 \tag{25}$$

where the equilibrium ratios K_i are defined by $K_i \equiv x_i/y_i$.

The equilibrium condition is described by a system of equations expressing the equality of chemical potentials in both phases:

$$h_i \equiv \mu_i(\mathbf{x}) - \mu_i(\mathbf{y}) = \ln K_i + \ln \Phi_i(\mathbf{x}) - \ln \Phi_i(\mathbf{y}) = 0, \quad i = 1, 2, ..., N \tag{26}$$

System (26), allowing for eqs 24 and 25, is a closed system for the determination of the total mole fractions of phases W_x and W_y and the phase concentrations x_i and y_i in the equilibrium state. Temperature and pressure are the independent variables of this problem.

3.2. Equation for Binodal Line as a Limiting Case of the Two-Phase Equilibrium. To determine the phase boundaries, we consider the limiting case where the infinitesimal new phase with composition **x** is derived from the source phase of composition **z** (hereafter **z** and **x** phases). The **x** phase differs from the phase **z** by its thermodynamic properties.

For the phase transition described by eqs 24−26, the change in the Gibbs free energy is

$$\Delta G = G^1 + G^2 - G^0 = \sum_{i=1}^{N} n_i^{(1)} \mu_i(\mathbf{x}) + \sum_{i=1}^{N} (n_i^{(0)} - n_i^{(1)}) \mu_i(\mathbf{y}) - \sum_{i=1}^{N} n_i^{(0)} \mu_i(\mathbf{z}) \tag{27}$$

Let

$$n_i^{(1)} = \epsilon_i, \qquad \sum_{i=1}^{N} \epsilon_i = \epsilon$$

where ϵ is an infinitesimal positive value. As follows from (24),

$$\lim_{L^{(1)} \to \epsilon} (y_i) = z_i + \sigma_{iy}(\epsilon) \qquad \lim_{L^{(1)} \to \epsilon} (x_i) = K_i z_i + \sigma_{ix}(\epsilon) \tag{28}$$

Consequently,

$$\lim_{L^{(1)} \to \epsilon} (\Delta G) = \epsilon \sum_{i=1}^{N} x_i \{\mu_i(\mathbf{x}) - \mu_i(\mathbf{z})\} \equiv \Delta G_\epsilon \tag{29}$$

where σ_{iy} and σ_{ix} are the errors of the order ϵ. It is evident that the problem is meaningless for $\epsilon = 0$ because the phase **x** is not determined. Therefore, the system properties must change abruptly on the binodal line.

Let us determine the function $F(\mathbf{x},T,P) \equiv \Delta G/\epsilon RT$, describing the change of the molar Gibbs phase-transition energy when composition **z** is fixed:

$$F(\mathbf{x},T,P) \equiv \frac{1}{RT} \sum_{i=1}^{N} x_i [\mu_i(\mathbf{x}) - \mu_i(\mathbf{z})] = \sum_{i=1}^{N} x_i [\ln x_i + \ln \Phi_i(\mathbf{x}) - \ln z_i + \ln \Phi_i(\mathbf{z})] \tag{30}$$

Equation 30 is the known formulation of the "tangential plane criterion" which describes the distance between the molar Gibbs energy surface and the tangent plane at a composition **z**. Equation 30 is widely used to solve various thermodynamic problems.[9−11]

In this work, eq 30 is used as a mathematical model for a two-phase boundary line (binodal) calculation.

Function $F(\mathbf{x},T,P)$ shows the distance from the energy surface to the tangent plane for every arbitrary $\mathbf{x}$. The tangent plane slope is determined by the chemical potentials of the components of phase $\mathbf{z}$. According to the phase-equilibrium conditions, described by an equality of chemical potentials of components in both phases, the equilibrium composition $\mathbf{x} = \mathbf{x}^*$ should also belong to this plane. It is evident that the function $F(\mathbf{x},T,P)$ must vanish at $\mathbf{x} = \mathbf{x}^*$ and $\mathbf{x} = \mathbf{z}$, whereas points $\mathbf{x}^*$ and $\mathbf{z}$ must be coordinates of two local minimums $F(\mathbf{x},T,P)$, according to the condition of the Gibbs free energy minimum at an equilibrium of phases. According to the equilibrium stability conditions, $F(\mathbf{x},T,P) > \mathbf{0}$ for $\mathbf{x} \neq \mathbf{x}^*$ and $\mathbf{x} \neq \mathbf{z}$.

Therefore, the problem of phase-boundary calculations will be formulated as a solution of the system

$$F(\mathbf{x},T,P) = 0 \tag{31}$$

$$\mathbf{h}(\mathbf{x},T,P) = 0 \tag{32}$$

$$Sx \equiv \sum_{i=1}^{N} x_i - 1 = 0 \tag{33}$$

and its subsequent analysis with respect to the performance of the stability conditions:

$$\det[\mathbf{h}_\mathbf{x}]_{\mathbf{x}=\mathbf{x}^*} > 0 \tag{34}$$

$$\det[\mathbf{h}_\mathbf{x}]_{\mathbf{x}=\mathbf{z}} > 0 \tag{35}$$

Vector-function $\mathbf{h}$ and matrix $\mathbf{h}_\mathbf{x}$ are determined as

$$h_i \equiv \partial F/\partial x_i = \ln x_i + \ln \Phi_i(\mathbf{x}) - \ln z_i - \ln \Phi_i(\mathbf{z}), \qquad i = 1, 2, ..., N$$

$$\mathbf{h}_x = [\partial h_i/\partial x_j], \qquad i = 1, 2, ..., N; \quad j = 1, 2, ..., N$$

According to the law of Gibbs' phase rule, phase boundaries have only 1 degree of freedom, and either P or T is independent. Therefore, the phase diagram (binodal line) on the T,P plane can be determined as a set of stable equilibrium states, $x_1^*(T_{b1}(P_{b1}))$, $x_2^*(T_{b2}(P_{b2}))$, ..., or $x_1^*(P_{b1}(T_{b1}))$, $x_2^*(P_{b2}^*(T_{b2}^*))$, ..., which satisfy eqs 31−33, when conditions (34) and (35) are fulfilled.

3.3. Homotopy Continuation Algorithm for Solving the Phase Boundary Calculation Problem. Homotopy continuation methods have become important in solving various chemical engineering problems when locally convergent methods fail.[12,13]

As mentioned early, the equations for the mathematical model of the binodal line are determined by system (31)−(33). Introducing new variables u_i, we obtain $x_i = u_i/Su$, where

$$Su = \sum_{i=1}^{N} u_i$$

Equations 31−33 can be rewritten in terms of the new variables:

$$F(\mathbf{u},T,P) = \sum_{i=1}^{N} u_i(\ln u_i + \ln \Phi_i(\mathbf{x}) - \ln z_i - \ln \Phi_i(\mathbf{z})) \tag{36}$$

$$h_i(\mathbf{u},T,P) = \ln u_i + \ln \Phi_i(\mathbf{x}) - \ln z_i - \ln \Phi_i(\mathbf{z}) = 0 \tag{37}$$

Let $\tilde{\mathbf{u}}$ be the vector of the solution of subsystem (37), that is, $h_i(\tilde{\mathbf{u}}) = 0$, where $i = 1, 2, ..., N$. Solutions exist at any arbitrary T and P values which do not belong to the binodal line. Substitution of $\tilde{\mathbf{u}}$ in eq 36 gives the residual

$$F(\tilde{\mathbf{u}},T,P) = -\ln Su(\tilde{\mathbf{u}}) \tag{38}$$

which can be either higher or lower than 0 at arbitrary values of T and P. The required coordinates of the binodal line are such solutions $-\tilde{\mathbf{u}}$, at which $-\ln Su(\tilde{\mathbf{u}}) = 0$; therefore,

$$\sum = 1, \qquad \tilde{\mathbf{u}} \equiv \mathbf{x}^* \tag{39}$$

To trace the homotopy path by integrating along the arc length, the Euler linear step predictor and Newton's correction method is applied.[12,13]

Let us consider the function in (38) and determine the sequence of temperature and pressure values that satisfy eq 39.

The solution is as follows. We set first the starting point T_0^k, P_0^k ($k = 0$) near the binodal with an "s"-type trajectory and check the condition $|F(T_0^k,P_0^k)| \leq \epsilon$, where k is the iteration number on the predictor step. When this condition does not hold, the starting values of T_0^k, P_0^k are corrected by several of Newton's iterations. As a result, one obtains the starting point T_b^0, P_b^0 on curve $\mathbf{s}$. One then singles out the direction parameter σ^k to be either $+1$ or -1, referring to the direction of further iterations.

The next point near trajectory "$\mathbf{s}$" is determined from the linear approximation:

$$T_0^{k+1} = T_b^k + \hbar^k \frac{dT}{ds}(s_k), \qquad P_0^{k+1} = P_b^k + \hbar^k \frac{dP}{ds}(s_k) \tag{40}$$

where $\hbar^k$ controls the length of an allowed step.

The derivatives dT/ds and dP/ds are the components of tangent vector $\sigma^k \bar{\mathbf{w}}\mathbf{s}$ at point T_b^0, P_b^0. The vector is normalized to unit length, and the direction is set by parameter σ^k. From the solution of equations

$$\begin{bmatrix} (\partial F/\partial T)(s_k) & (\partial F/\partial P)(s_k) \\ 0 & 1 \end{bmatrix} \times \begin{bmatrix} w_1 \\ w_2 \end{bmatrix} = \begin{bmatrix} 0 \\ 1 \end{bmatrix} \tag{41}$$

one finds vector $\mathbf{w}$, which can be normalized as

$$\bar{w}_1 = \frac{w_1}{||\mathbf{w}||_2}, \qquad \bar{w}_2 = \frac{w_2}{||\mathbf{w}||_2} \tag{42}$$

Therefore,

$$\frac{dT}{ds}(s_k) = \sigma^k \bar{w}_1^k, \qquad \frac{dP}{ds}(s_k) = \sigma^k \bar{w}_2^k \tag{43}$$

If the absolute value of dF/dT in system (41) is lower than $\epsilon_{sing} \approx 10^{-3}$ to 10^{-2}, one does not solve system (41), but rather a similar system obtained by the substitution of vector $|1, 0|$ for the bottom matrix line.

Using subscript "0" for T and P in formula (40), we note that these values are in close proximity to the binodal line (but not on the binodal line) and serve as initial approximations for the Newton procedure at each $k + 1$ step of the predictor.

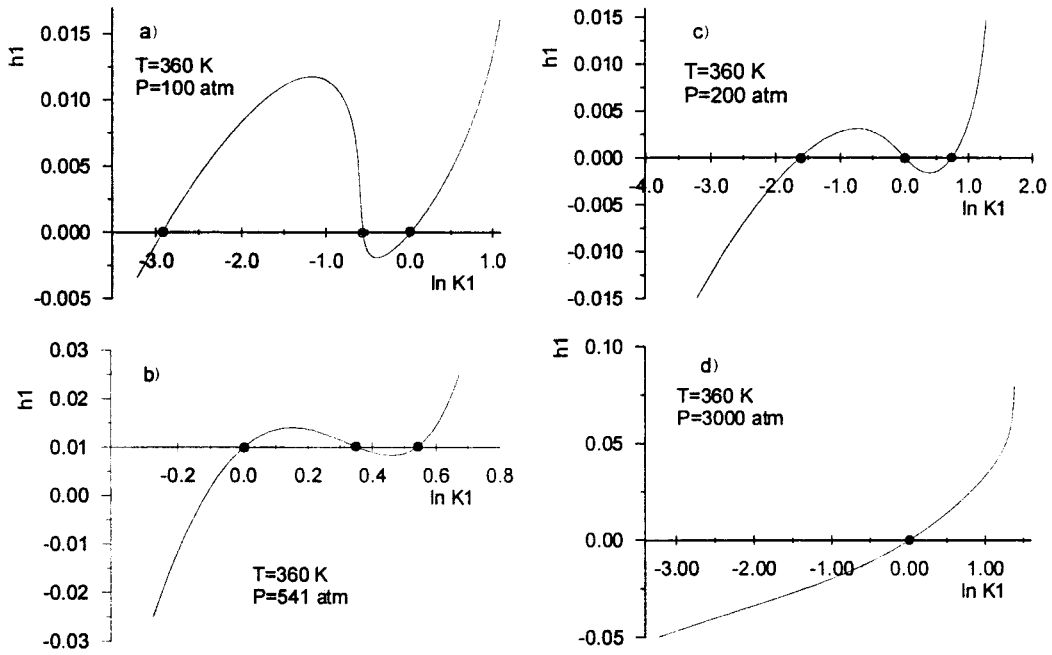

Figure 3. (a−d) Function $h_1 = \partial F(\mathbf{u})/\partial u_1$ vs $\ln K_1 = \ln(u_1/z_1)$, for a binary mixture N_2-NH_3. Index "1" denotes nitrogen. The points $h_1 = 0$ correspond to three points of function F (36) extrema. Heavy points, minima points; light points, maxima points.

The adjustment of T_0^{k+1}, P_0^{k+1} is as follows. Let i be the number of iterations by the Newton method at the $k + 1$ step of the predictor. The sequence of the adjustment steps is determined from the solution of the system as

$$\begin{bmatrix} (\partial F/\partial T)(T_i^{k+1},P_i^{k+1}) & (\partial F/\partial P)(T_i^{k+1},P_i^{k+1}) \\ (\mathrm{d}T/\mathrm{d}s)(s_k) & (\mathrm{d}P/\mathrm{d}s)(s_k) \end{bmatrix} \times \begin{bmatrix} \Delta T_i^{k+1} \\ \Delta P_i^{k+1} \end{bmatrix} = \begin{bmatrix} -F(T_i^{k+1},P_i^{k+1}) \\ 0 \end{bmatrix} \quad (44)$$

$$T_{i+1}^{k+1} = T_i^{k+1} + \Delta T_i^{k+1}, \qquad P_{i+1}^{k+1} = P_i^{k+1} + \Delta P_i^{k+1} \quad (45)$$

Adjustment is performed until the condition $|F| \le \epsilon$ is fulfilled (ϵ is the preset accuracy). The T_b^{k+1} and P_b^{k+1} values determine a new point on the binodal line.

To avoid many unnecessary steps and to take care that the solution is not drifting away from the curve, the algorithm provides automatic control of step size by choosing parameter $\hbar^k$. The sign of parameter σ^k is also checked upon the predictor iterations.[12]

3.4. Problems of Existence and Uniqueness of a Solution. To calculate F (eq 38), it is necessary to solve the nonlinear system (37) at each iteration. We used both the Newton method and the direct substitution method. In some cases where the matrix $[\partial h_i/\partial u_j]$ is ill-conditioned, the latter method is more reliable and robust. As a result, the direct substitution method is preferred, despite the larger number of iterations required.

Consider now the features of the solution of system (37). As is known,[9] the Gibbs's free energy surface in the composition space has R local minima, corresponding to R equilibrium phases. In practice, heterogeneous systems usually contain no more than three phases at a time, that is, two liquids and one vapor-gas phase. The number and nature of phases depend on the temperature, pressure, and chemical composition of the initial mixture. Close to the binodal line, function (36) should have no more than two local minima. Moreover, according to the formulated problem, coordinates of one minimum must coincide with composition $\mathbf{z}$. Such "trivial" $\tilde{\mathbf{u}} = \mathbf{z}$ solution of system (37) is one of the true solutions of problem.

The other local minimum of function (36) must be consistent with the solution $\tilde{\mathbf{u}} \neq \mathbf{z}$, corresponding either to a "strained" equilibrium composition $\tilde{\mathbf{x}}$, if $Su(\tilde{\mathbf{u}}) \neq 1$, or a true equilibrium composition $\mathbf{x}^*$, if $Su(\tilde{\mathbf{u}}) = 1$.

We have numerically studied the problem (37) using model mixtures of different compositions. The main results will be illustrated using particular examples. As an illustrative example, a binary system containing N_2 ($z_1 = 25\%$) and NH_3 ($z_2 = 75\%$) has been chosen.

Figure 3a−d presents the $h_1-\ln(K_1)$ plots, where $K_1 = u_1/z_1$ and $h_1 = \partial F(\mathbf{u})/\partial u_1$. According to Figure 3a−c, $h_1 = 0$ vanishes three times, which corresponds to three extrema of function (36). One of the intersection points ($h_1 = 0$) corresponds to maximum F, and the other two points correspond to local minima. One of the minima (Figure 3a,b) fits the composition $\mathbf{z}$ ("trivial" solution, $\ln K_1 = 0$), and the coordinates of the other minimum is a desired solution, $\tilde{\mathbf{u}} \neq \mathbf{z}$. In these cases (Figure 3a,b), the chosen parameters T,P are near the binodal line.

In Figure 3c, the trivial solution $\tilde{\mathbf{u}} = \mathbf{z}$ is a maximum of F. This means that the initial mixture with composition $\mathbf{z}$ is thermodynamically unstable and divides into two phases whose compositions are given by coordinates $\ln K_1^{(1)} = \ln(\tilde{u}_1^{(1)}/z_1)$ and $\ln K_1^{(2)} = \ln(\tilde{u}_1^{(2)}/z_1)$ of the other two intersection points of the curve h_1 and x axis which denote two local minima of function F. Consequently, the chosen parameters T,P (Figure 3c) are not near the binodal line. These belong to the two-phase region.

Figure 3d illustrates the situation when a mixture $\mathbf{z}$ is thermodynamically stable at a given T,P. Function F has only one extremum which is a stable minimum with the $\tilde{\mathbf{u}} = \mathbf{z}$ coordinates.

Note the position of the desired solution with respect to the trivial one (Figure 3a,b). In the first case, the solution is to the left and in the second to the right of the trivial solution. It is obvious that the desired

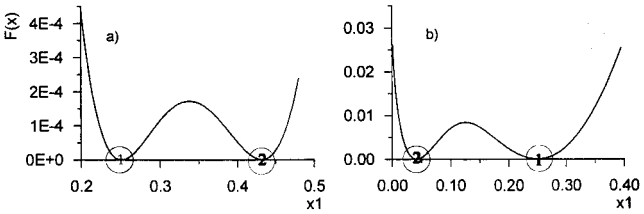

Figure 4. (a, b) Function $F(\mathbf{x})$ (eq 31) for a binary mixture of N_2−NH_3. "1" denotes the given composition $z_1 = 0.25$, $z_2 = 0.75$. "2" denotes the desired equilibrium composition: (a) $x_1 = 0.4335$, $x_2 = 0.5665$, $\rho_x = 401.6$ g/L, $\rho_z = 427.6$ g/L, $T = 360.4$ K, and $P = 541.3$ atm. (b) $x_1 = 0.0415$, $x_2 = 0.9585$, $\rho_x = 314.8$ g/L, $\rho_z = 142.9$ g/L, $T = 383.2$ K, and $P = 148.9$ atm.

stationary points will be found by the iterative procedure only if a correct choice is made for the initial $\mathbf{u}_0$ approximations.

We have shown that the iterative convergence is always guaranteed to find the nontrivial solution $\mathbf{u} \neq \mathbf{z}$, if the initial approximations $\mathbf{u}_0$ meet the following conditions:

$$S^0 \equiv \sum_{i=1}^{N} z_i/K_1^0 \gg 1 \qquad \text{where } K_1^0 = \tilde{u}_{i0}/z_i \quad (46)$$

As initial approximations u_{i0} at the $k+1$ iteration of the predictor, one chooses x_i values found at the kth step, if these approximations satisfy condition (46). A good estimation of u_{i0} is otherwise obtained by[14]

$$K_i^0 \equiv \frac{u_{i0}}{z_i} = \frac{P_{ci}}{P} \exp\left[5.3727(1+\omega_i)\left(1 - \frac{T_{ci}}{T}\right)\right] \quad (47)$$

or by the reverse value $K_i^0 = 1/K_i^0$.

In Figure 4a,b, function $\mathbf{F}(\mathbf{x})$ versus x_1 is shown for T,P occurring directly on the binodal line. Building similar construction of an F surface in the space of $\mathbf{x}$ compositions is a problem of calculating a binodal line for a multicomponent mixture. For the parameters given in Figure 4a, $\mathbf{z}$ is the denser phase and $\mathbf{x}$ the lighter phase. In Figure 4b, the situation is reversed. The T value is increased and the P value is decreased, point "2", moving along the binodal line in the direction of the mixture critical point. This point is a singular point and cannot be attained by the algorithm described above.

4. Critical State Criterion of a Multicomponent Mixture

Gibbs classical theory of critical points lead to two nonlinear equations in the intensive variables:[6,15]

$$F_1(T,P) = \mathrm{Det}(\mathbf{M}_1) = 0 \quad (48)$$

$$F_2(T,P) = \mathrm{Det}(\mathbf{M}_2) = 0 \quad (49)$$

Elements of matrix $\mathbf{M}_1$ are the second derivatives of the Gibbs free energy:

$$\mathbf{M}_1 = \left\{\frac{\partial^2 G}{\partial z_i \partial z_j}\right\} = \left\{\frac{\partial \mu_i(\mathbf{z})}{\partial z_j}\right\}, \quad i = 1, 2, ..., N, \quad j = 1, 2, ..., N \quad (50)$$

Matrix $\mathbf{M}_2$ is derived from $\mathbf{M}_1$ by substituting the row vector for any matrix row as

$$[\partial F_1/\partial z_1,\ \partial F_1/\partial z_2,\ ...,\ \partial F_1/\partial z_N] \quad (51)$$

If only eq 48 is met, the set of temperature−pressure pairs forms a *spinodal* line, or a stability limit line on either the T,P or on the P,V planes.[9,16] The spinodal line separates the region of possible metastable equilibrium from the region where the mixture is absolutely unstable and metastable states are impossible.

The simultaneous fulfillment of eqs 48 and 49 determines the mixture critical point coordinates T_c,P_c.

Calculations of the critical point, based on the direct solution of eqs 48 and 49, are "rigorous", and the obtained data agree well with experimental results.[15] However, these equations are of such complexity as to discourage application to large systems. In the standard approach, as employed by Peng and Robinson,[15] it is necessary to find $3(N^2 - 2N + 3)$ determinants of the order $(N-1)$ at each test point merely to evaluate the functions.

In this paper we suggest a simpler system of equations for the critical phase, which preserves all basic properties of the rigorous model (48)−(49).

Consider the N components of a homogeneous mixture with composition $\mathbf{z}_0$. Let $\mu_i(\mathbf{z}_0)$ stand for the chemical potential of the ith component, calculated at some fixed T and P values. The function $\mu_i(\mathbf{z})$ may be approximated by expansion into a Taylor series around the test point $\mathbf{z}_0$.

$$\mu_i(\mathbf{z}) = \mu_i(\mathbf{z}_0) + \sum_{j=1}^{N} \frac{\partial \mu_i}{\partial z_j} \Delta z_j + \frac{1}{2} \sum_{k=1}^{N} \sum_{j=1}^{N} \frac{\partial^2 \mu_i}{\partial z_k \partial z_j} \Delta z_j \Delta z_k + 0(\Delta z^3), \quad i = 1, 2, ..., N \quad (52)$$

Derivatives in the right part of eq 52 are calculated at $\mathbf{z} = \mathbf{z}_0$, and Δz_j,Δz_k denote the vector elements as

$$\Delta \mathbf{z} = [z_1 - z_{1,0},\ z_2 - z_{2,0},\ ...,\ z_N - z_{N,0}] \quad (53)$$

Summing eq 52 by index i with weights Δz_i, one has

$$S \equiv \sum_{i=1}^{N} \Delta \mu_i \Delta z_i = \sum_{i=1}^{N} \sum_{j=1}^{N} \frac{\partial \mu_i}{\partial z_j} \Delta z_j \Delta z_i + \frac{1}{2} \sum_{i}^{N} \sum_{k}^{N} \sum_{j}^{N} \frac{\partial^2 \mu_i}{\partial z_k \partial z_j} \Delta z_i \Delta z_k \Delta z_j + 0(\Delta \mathbf{z}^4) \quad (54)$$

where $\Delta \mu_i = \mu_i(\mathbf{z}) - \mu_i(\mathbf{z}_0)$.

The right-hand part of eq 54 is an approximation of the fundamental Gibbs relation of the second differential of the internal energy.[9] When T and P are constant, eq 54 approximates the second differential of the Gibbs free energy function.

At predetermined pressure and temperature the homogeneous mixture of $\mathbf{z}_0$ is thermodynamically stable if function S is positive at any arbitrary variations of composition near $\mathbf{z}_0$. The limits of mixture stability are T and P values, at which the quadratic form in the right-hand part of eq 54 is positive semidefinite. A set of values $(T_{sp,1},P_{sp,1})$, $(T_{sp2},P_{sp,2})$, ..., satisfying the condition

$$S_1 \equiv \sum_{j=1}^{N} \sum_{i=1}^{N} \frac{\partial \mu_i(\mathbf{z}_0)}{\partial z_j} \Delta z_i \Delta z_j = 0 \quad (55)$$

form a spinodal line on the T,P plane.

The critical point T_c,P_c of a mixture is a marginally stable point in the spinodal line.[9] At this point, if condition (55) is met, the following conditions must also be satisfied:

$$S_2 \equiv \sum_i^N \sum_k^N \sum_j^N \frac{\partial^2 \mu_i}{\partial z_k \partial z_j} \Delta z_i \Delta z_k \Delta z_j = 0 \qquad (56)$$

Equations 55 and 56 are taken as the bases of the "critical phase" model.

4.1. Calculation of a Spinodal Line. Consider first the trajectory of the successive solutions ($T_{sp,1}$,$P_{sp,1}$), ($T_{sp,2}$,$P_{sp,2}$), ..., satisfying eq 55 at the preset mixture composition $\mathbf{z}_0$.

Function (55) may be rewritten in the matrix form

$$S_1 \equiv \Delta \mathbf{z}^T \mathbf{H} \Delta \mathbf{z} \qquad (57)$$

where $\mathbf{H}$ is the symmetric matrix as

$$h_{ij} = \frac{\partial \ln f_i(\mathbf{z})}{\partial z_j}, \qquad i = 1, 2, ..., N; \quad j = 1, 2, ..., N \qquad (58)$$

whose elements are calculated at $\mathbf{z} = \mathbf{z}_0$.

Using the well-known methods of linear algebra, matrix $\mathbf{H}$ may be transformed to the diagonal form

$$\mathbf{U}^T \mathbf{H} \mathbf{U} = \mathbf{L}, \qquad \mathbf{H} = \mathbf{U} \mathbf{L} \mathbf{U}^T \qquad (59)$$

where $\mathbf{L} = \mathbf{diag}(\lambda_i)$, λ_i are the eigenvalues of $\mathbf{H}$, and $\mathbf{U}$ is the orthogonal matrix of eigenvectors $\mathbf{u}$ of matrix $\mathbf{H}$. By orthogonality of $\mathbf{U}$, these vectors satisfy the following conditions:

$$\mathbf{u}_i^T \mathbf{u}_j = 0 \text{ at } i \neq j; \qquad \mathbf{u}_i^T \mathbf{u}_j = 1 \text{ at } i = j \qquad (60)$$

Let us determine the principal components $\Delta\psi_i$ as a new system of variables:

$$\Delta \psi_i = \mathbf{u}_i^T \Delta \mathbf{z} = \sum_{j=1}^N u_{ij} \Delta z_j, \qquad i = 1, 2, ..., N \qquad (61)$$

and rewrite function (57) in a new coordinate system:

$$S_1(\mathbf{z}_0, T, P) = \sum_{i=1}^N \lambda_i \Delta \psi_i^2 = 0 \qquad (62)$$

Let $\mathbf{u}_m$, the eigenvector of $\mathbf{H}$, correspond to the smallest eigenvalue λ_m. The principal component $\Delta\psi_m$ will be

$$\Delta \psi_m = u_{m,1} \Delta z_1 + u_{m,2} \Delta z_2 + ... + u_{m,N} \Delta z_N \qquad (63)$$

If the variations of Δz_i are chosen so that $\Delta z_i = \xi u_{m,i}$, where ξ is an arbitrary scalar multiplier (for example, $\xi = 1$), then according to (60), $\Delta\psi_m = 1$,$\Delta\psi_j = 0$ ($j = 1, 2, ..., N$; $j \neq m$), and eq 62 becomes

$$S_1(\mathbf{z}_0, T, P) \equiv \lambda_m(T, P) = 0 \qquad (64)$$

It is evident that S_1 vanishes at $\lambda_m \to 0$. Therefore, the problem reduces to an evaluation of the T,P values at which $\lambda_m(T,P) = 0$. Because at a fixed mixture composition the degree of freedom along the spinodal line is 1, the desired values of T and P form dependent pairs of parameters.

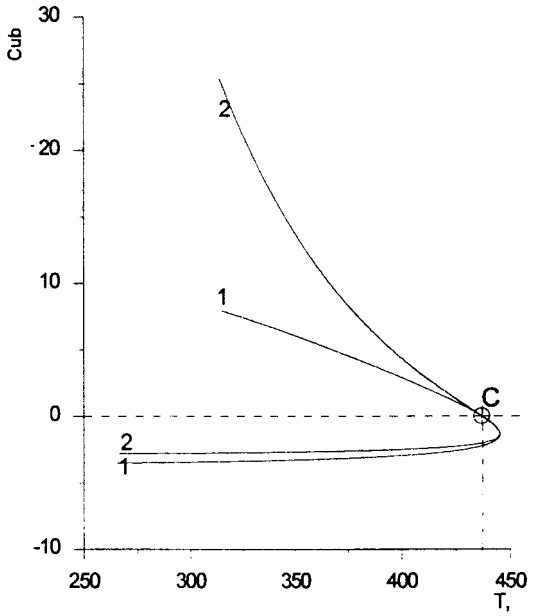

Figure 5. Graphics of "cubic form", calculated using different models. Curve 1 calculations by eqs (64) and (65); curve 2 calculations by eqs (48) and (49). "**C**" denotes the critical point.

Taking into account the above discussion, the second equation for the critical phase may be presented as

$$S_2(\mathbf{z}_0, T, P) \equiv \sum_{i=1}^N \frac{\partial \lambda_m}{\partial z_i} u_{m,i} = 0 \qquad (65)$$

Equations 64 and 65 are equivalent to eqs 55 and 56. A simultaneous fulfillment of equalities (64) and (65) determines T_c,P_c coordinates of the mixture critical point.

Using the above homotopy continuation algorithm, and replacing function F with function S_1 in eqs 41−44, one solves eq 64. So algorithm (41)−(44) is the standard unit in the reactor modeling software. Elements of matrix $\mathbf{H}$ are normalized by the corresponding substitution of variables. Then, matrixes $\mathbf{L}$ and $\mathbf{U}$ are found by the Jacobi method, and partial derivatives $\partial\lambda_m/\partial z_i$ in eq 65 are calculated by numerical differentiation.

4.2. Localization of a Critical Point. In the course of iteration, function S_2 is determined only at points where eq 64 is fulfilled. Moving along the spinodal curve, one determines $T_{sp,L}$,$P_{sp,L}$, $T_{sp,R}$,$P_{sp,R}$ values, between which function S_2 changes its sign. Thereafter, the T_c,P_c values are found with high accuracy by Newton's method.

5. Phase Behavior of Multicomponent Mixtures

5.1. Critical Point, Calculated and Experimental Data. The critical point of a multicomponent mixture of a given composition is one of the most important and necessary characteristics of a technological process performed in the reactor under near- or supercritical conditions. Therefore, it is important to compare our results with the reference data.[8,15,16]

Figure 5 illustrates the "cubic" forms calculated by eq 49 (curve 2) and eq 65 (curve 1), respectively. The model mixture has the following composition (mole factions): CH_4, 0.4590; C_2H_9, 0.1315; C_3H_8, 0.0830; n-C_5H_{12}, 0.1314; n-C_7H_{16}, 0.1925.

Table 3. Coordinates of the Critical Point of a Methane Mixture

	this work	Michelsen[8]	Peng and Robinson[15]	Heidemann and Khalil[16]	expt.[15]
T_c, K	202.77	203.13	202.44	202.20	201.09
P_c, atm	59.20	58.11	59.04	58.89	55.78

Table 4. Coordinates of the Critical Point of the CO_2−*n*-C_4H_{10} Mixtures

mole fraction of C_4H_{10}	this work, calc		Peng and Robinson, calc[15]		exp[15]	
	T_C, K	P_C, atm	T_C, K	P_C, atm	T_C, K	P_C, atm
0.1694	328.77	76.85	326.8	77.43	325.90	76.28
0.3334	352.65	82.78	356.30	81.50	351.7	81.70
0.4984	380.70	76.58	381.70	74.28	377.20	75.36
0.6740	401.21	62.98	401.50	61.31	398.8	62.81
0.8273	411.27	53.31	414.30	49.73	412.3	51.09

It is obvious that the curves obtained by different models are different. However, the coordinates of the critical mixture point coincide completely. In this case, the calculated critical point coordinates are $T_c = 436.933$ K and $P_c = 119.389$ atm.

The next example concerns the following model mixture: CH_4, 0.9430; C_2H_6, 0.0270; C_3H_8, 0.0074; *n*-C_4H_{10}, 0.0049; *n*-C_5H_{12}, 0.0010; *n*-C_6H_{14}, 0.0027; N_2, 0.0140. This model mixture is used for comparative analysis in a number of works.[8,15,16] The experimental critical parameters of this mixture are given in ref 15.

Table 3 presents calculated and experimental parameters of the critical point.

Heidemann et al.[16] and Michelsen[8] use different models of the critical phase. The mixture $P-V-T$ properties were calculated by the SRK equation without allowance for binary coefficients k_{ij} and c_{ij}. Therefore, we do not use these corrections in this example. Peng and Robinson[15] used model (48)−(49) and the P−R equation of state. They did not report on the use of any corrections.

As shown in Table 3, the results obtained for different models agree well. It is well-known that, without k_{ij} and c_{ij} corrections, the SRK equation somewhat overestimates values of the critical pressure compared to the experimental data. This is also the case here.

The next example is used for comparison between the calculations and experimental data as well as comparison with the data calculated in ref 15 using a "rigorous" model of (48)−(49) and the P−R equation of state. Binary mixtures of *n*-butane and carbon dioxide are considered (Table 4). In this example we used k_{ij} and c_{ij} corrections.

Table 5. Composition of the Mixed Fractions

species	fraction A	fraction B
methane	0.156	0.762
ethane	0.111	0.152
propane	0.108	0.058
n-butane	0.246	0.022
n-heptane	0.379	0.006

Table 6. Model Mixture: Mole Fractions and Physical Properties of Components

species	formula	mole fraction	T_c, K	P_c, atm
nitrogen	N_2	0.03	126	33.5
carbon dioxide	CO_2	0.05	304	72.8
ammonia	NH_3	0.73	406	111
water	H_2O	0.02	647.3	218
toluene	C_7H_8	0.10	562	48.3
4-methylpyridine	C_6H_7N	0.05	699	52.4
benzaldehyde	C_7H_6O	0.01	699	41.6
1-methylnaphthalene	$C_{11}H_{10}$	0.01	789	38

According to Table 4, the data obtained by different models deviate within the limits of experimental error. As was noted above, our model is more efficient regarding the calculation procedure.

Composition dependencies of the critical temperatures (Figure 6a) and critical pressures (Figure 6b) were calculated for mixtures prepared by the mixing of fractions A and B[15] (see Table 5). The molar fraction of **A** is plotted on the *x* axis, and the calculated critical parameters obtained by eqs 64 and 65 and by a "rigorous" model[15] are plotted on the *y* axis.

The points show a good agreement between the results. Note that the critical temperature changes monotonically with the changing **A** fraction. The critical pressure passes a maximum, which is greater than the critical pressure for either pure component. This phenomenon has been observed and systematically studied for many binary systems.

5.2. Phase Diagrams and the Phase-Transition Features. 5.2.1. Model Mixture with a Supercritical Solvent. Table 6 presents the composition (mole fractions) and physical properties of the individual components considered.

Now we shall consider the areas of mixture stability and their mutual arrangement on the $P-V$ plane. The phase diagram of the model mixture in $P-V$ coordinates is shown in Figure 7.

Contour I corresponds to a bimodali line, contour II corresponds to the spinodal line, and "**C**" is the critical mixture point. The $P-V$ isotherms are represented by dotted lines, which are calculated by the SRK EOS,

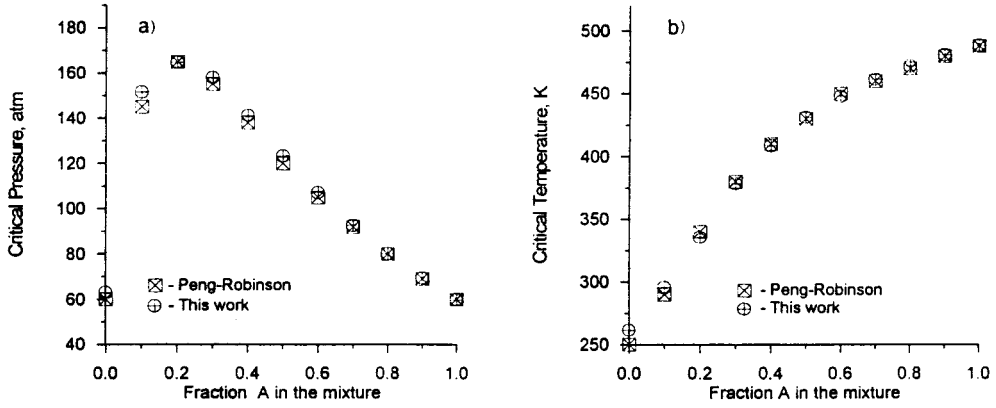

Figure 6. (a, b) Critical pressure and critical temperature vs fraction **A** in the mixture.

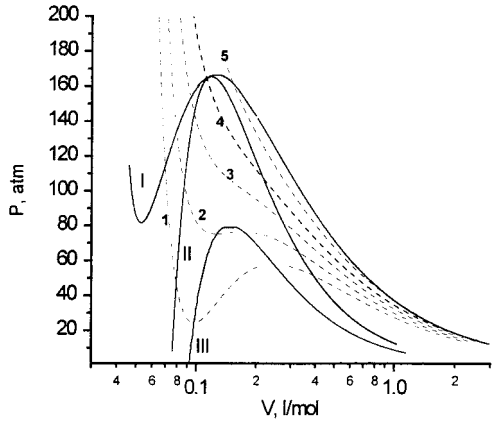

Figure 7. $P-V$ diagrams for a model mixture isotherms. T, K: (1) 400, (2) 425, (3) 450, (4) 472, critical, and (5) 500.

and line III connects the extreme's points, in which $dP/dV = 0$. The area between contours I and II represents the area where metastable states of the mixture are possible. The supercooled vapor states can be realized to the right of a critical point between I and II, and to the left, the condition of the preheated liquid. The area inside contour II is the area of diffusion instability of the mixture, where metastable states are impossible, and the mixture of overall composition **z** cannot exist. The area, determined by line III, is the area of mechanical instability of the mixture. From Figure 7 it follows that when we move on any isotherm, the diffusion instability of a mixture comes before a mechanical instability. This phenomenon takes place just for the multicomponent mixtures, while for pure components areas II and III coincide. As shown on the diagram in Figure 7, along the mixture critical isotherm the condition of mechanical stability is realized.

The peculiarities of phase behavior for the above mixture are in many respects common for other mixtures in which a component plays the role of solvent (in this case ammonia). This "near-critical area", which lies between the critical parameters of pure ammonia (T_c = 406 K and P_c = 111 atm) and the critical point of the mixture (T_c = 472.2 K and P_c = 164.2 atm), has a unique set of properties (low viscosity, high diffusivity, and high solubility of gases in liquid phase), which provide the advantages of the supercritical technologies.

Similar phase diagrams are typical for hydrocarbon mixtures containing, for example, a large amount of methane[7,8] and for working mixtures obtained at separate stages of the Fischer−Tropsch synthesis. When the process is carried out under "supercritical" conditions, one of the reaction products, propane[19] or hexane,[20] is used usually as a solvent.

The yield of the equilibrium phases and their composition, determined from eqs 24−26 at preset T and P in the region enclosed by binodal lines, are very important for the characterization of mixture phase composition in the reactor. Let us discuss these features. The yield of the more dense phase (condensate) versus pressure at different isotherms is shown in Figure 8.

It is of interest to note how the condensate yield changes depending on the isotherm position relative to the critical mixture point. At $T \geq 493$ K, the isotherms situated to the right of the critical point exhibit some retrograde phenomena.[9] Under isothermal compression, the condensate of a mixture begins to form when the pressure reaches a value of $P_{b,1}$. As the pressure rises, the condensate fraction passes a maximum and vanishes at $P_{b,2}$. At this point the mixture becomes a homogeneous compressed gas. Krichevskii[6] was the first to establish the retrograde evaporation caused by a nonlinear dependence between pressure and the solubility of the high-boiling components in the compressed gases. The retrograde evaporation is also characteristic of hydrocarbon mixtures containing individual components with a wide spectrum of critical parameters, among them supercritical, near-critical, and undercritical components.

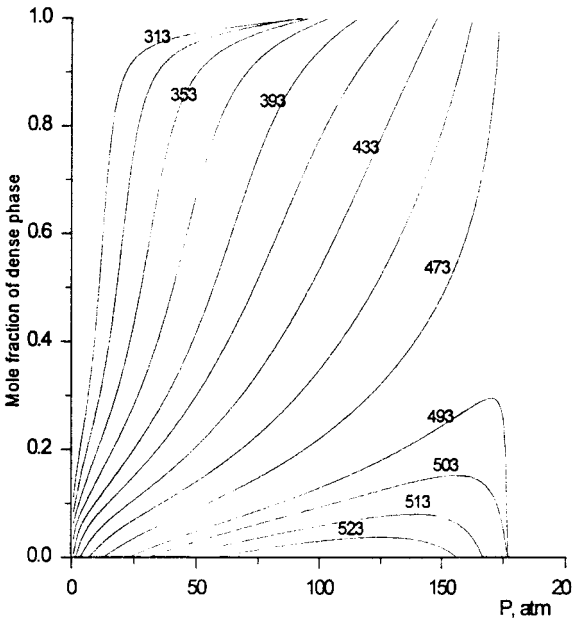

Figure 8. Mole fractions of a denser phase (condensate) in an equilibrium state vs pressure at different temperatures. Numbers in the curves denote the temperature, K.

Table 7. Composition (mol %) and Properties of Equilibrium Phases: T = 406 K, P = 111 atm

species	phase 1	phase 2
N_2	2.403	14.259
CO_2	4.791	8.944
NH_3	73.017	72.673
H_2O	2.071	0.662
C_6H_7N	5.253	0.228
C_7H_8	10.363	3.164
C_7H_6O	1.050	0.051
$C_{11}H_{10}$	1.052	0.019
W	94.961	5.039
ρ, g/L	456.24	115.59

In Figure 8, for the isotherm at T = 473 K, which is very close to the critical mixture temperature, the yield of a more dense phase increases sharply with the increasing pressure and the two-phase state disappears abruptly. In isotherms at lower temperatures (T < 433 K), a two-phase mixture consists predominantly of the liquid phase, which increases monotonically with the increasing pressure.

As mentioned above, the near-critical $P-V$ region which begins at critical parameters of ammonia and ends at the mixture critical point is very interesting for the chemical processes. Table 7 presents the phase split characteristics at the critical parameters of ammonia. Phase compositions are distinguished by approximately equal parts of the solvent between both phases. Along with the solvent, one phase contains predominantly light gases, while the other contains high molecular weight organics. Such a phase distribution (Table 7) is

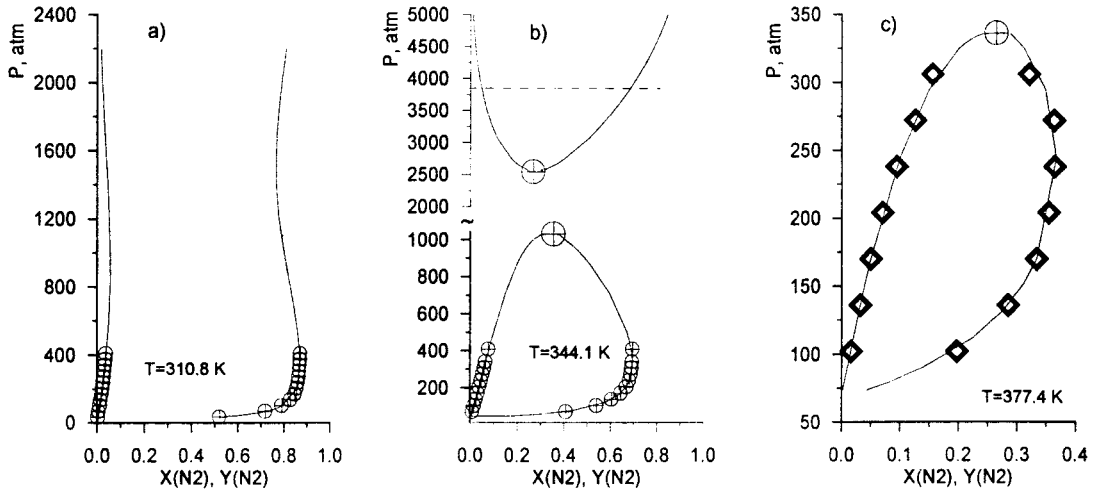

Figure 9. (a–c) "Pressure–composition" diagrams of the N_2–NH_3 mixtures.

typical for the whole near-critical region, but phase yields change with respect to temperature and pressure.

5.2.2. "Gas–Gas" Equilibrium. The phenomenon of limited solubility of fluids in the super-high-pressure region was first observed for binary nitrogen–ammonia mixtures of various compositions. van der Waal first proposed the possibility of a "gas–gas" equilibrium. Krichevskii supported this proposal with the experimental data[6] and explained qualitatively this phenomenon.

In this work we made an attempt to describe the gas–gas equilibrium using the SRK EOS. Figure 9a–c shows phase diagrams of "pressure–composition" for binary N_2–NH_3 mixtures at 310.8, 344.1, and 377.4 K. The solid lines stand for calculations with a model, and individual symbols stand for the experimental data.[6]

In the low-temperature region (Figure 9a), the two branches of the phase equilibrium diagram run almost parallel and do not merge together at the critical point with the increasing pressure up to 2200 atm. The right branch shows the maximum of ammonia solubility in compressed nitrogen at $P \approx 1400$ atm, and the left branch shows the maximum of nitrogen solubility in liquid ammonia at $P \approx 1000$ atm.

The phase diagram changes significantly as the temperature increases. At $T = 344.1$ K and $T = 777.4$ K (Figure 9 b,c) the right and left branches come close and merge together at the critical points ($P \approx 1000$ atm at $T = 344.1$ K and $P \approx 350$ atm at $T = 377.4$ K).

As shown in Figure 9b, the monophase condition over critical pressure holds at a pressure interval 1000–2500–2600 atm. At higher pressures the homogeneous supercritical fluid splits again into two phases; that is, the gas–gas equilibrium takes place. The gas–gas equilibrium lines with a critical point at $P \cong 2500$ atm were calculated by RKS EOS. They describe well the regularities observed in experiments.[6] Yet, at $T = 377.4$ K (Figure 9c), we did not succeed in simulating a gas–gas equilibrium because the experimental data were not sufficient for calculations of the binary interaction coefficients.

The gas–gas equilibrium is also observed in nitrogen–*n*-heptane binary mixtures (Figure 10).

A S-shaped binodal line in the $P-T$ diagram obtained for a mixture of 70% N_2/30% C_7H_{16} divides the phase plane into homogeneous (I) and heterogeneous (II) regions; "*C*" is the critical point. The calculated coordinates of *C* ($P = 300.5$ atm and $T = 453$ K) agree well with the experimental data.[21] The line of the gas–liquid equilibrium goes along the bottom branch and smoothly transforms into the gas–gas equilibrium at *C*, which is observed at high pressure and temperature, exceeding the critical temperature of *n*-heptane.

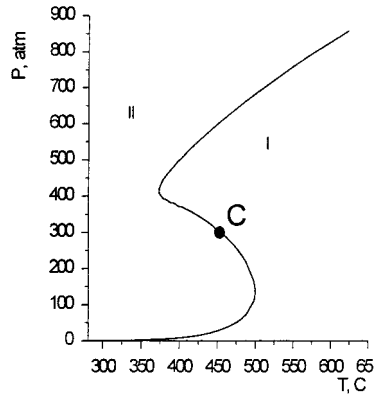

Figure 10. $P-T$ phase diagram of the N_2–*n*-C_7H_{16} mixtures.

In Figure 10, the "liquid–gas" phase diagrams are shown in the pressure–composition coordinates (bottom part) at $T = 453$ K (curve 1) and 497 K (curve 2). Symbols denote the experimental data,[21] and solid lines denote model calculations. The letter "*C*" indicates critical points.

The curves for the gas–gas equilibrium were calculated at 453 and 553 K (Figure 11, curves 1′ and 2′). Circles show critical points. Note that the curves of the gas–gas equilibrium are nearly symmetric with respect to the critical composition (45% N_2, 55% C_7H_{16}). In Figure 11 (top), the left branches exhibit nitrogen solubility in supercritical heptane and the right branches show heptane solubility in supercritical nitrogen. As the pressure increases to 900–1000 atm, the mutual solubility of the components drops and the composition of each phase tends to a pure component. Such behavior of the gas–gas equilibrium curves has been observed experimentally in some other systems.[6]

The above examples illustrate the potentials of the SRK EOS for modeling almost all of the experimentally observed high-density equilibrium phenomena. Such high-density phase separations are important in various applications, one of which we will discuss in the following section.

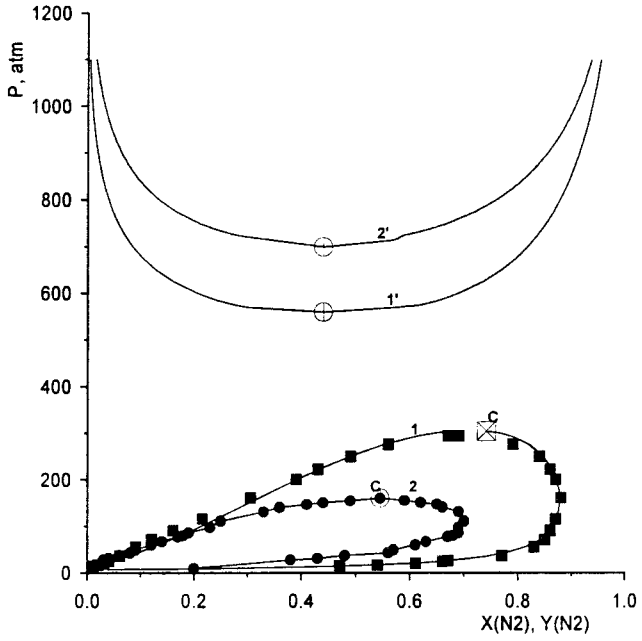

Figure 11. $P-x$ phase diagrams of the N_2-n-C_7H_{16}.

6. Fischer–Tropsch Process in a Slurry Reactor

The chemistry of the Fischer–Tropsch (FT) synthesis involves the hydrogenation of carbon monoxide, in which a broad spectrum of products including paraffins (alkanes), olefins (alkenes), alcohols, aldehydes, ketones, and so forth are produced. The FT slurry reactor is a multiphase system of a solid catalyst, liquid products, and gas-phase reactants. Under reaction conditions the chemical reactions are accompanied by phase conversions. Using this process as an example, we may discuss some general problems encountered in modeling reactors with modeling involving phase transitions. The catalytic process occurring in the reactor determines the choice of the main technological stages that directly interact with the reactor. Therefore, in choosing the optimal process parameters, the whole reactor unit as a part of the general process scheme must be calculated.

We would like to discuss briefly the literature data related to the Fischer–Tropsch (FT) process. Saxenna[22] has reviewed the publications dedicated to mathematical modeling of three-phase reactors, including the slurry reactors for FT synthesis. The list of cited publications includes 258 works published since 1950 until 1993. The review concerns a large number of problems, including hydrodynamics, heat and mass transfer, and mathematical models for FT synthesis. Different concepts on mathematical modeling of FT processes in a slurry reactor are discussed and experimental results obtained by different authors are compared.

Regarding the FT process, the general assumptions are as follows:

(1) The suspension phase is perfectly back-mixed, the catalyst is uniformly distributed in the liquid, and the gradients of concentration and temperature for the liquid phase are not found.

(2) The slurry reactor is at steady state, implying that thermodynamic equilibrium exists with respect to various states variables in each of the individual phases as well as at the interfaces of two different phases. The steady-state operation also implies that there is no product accumulation in the reactor.

At the same time the following problems were not properly reflected in the known models of the FT slurry reactor:

(1) Complex composition of the reaction mixture.

(2) Complex reaction kinetic.

(3) Phase transitions in multicomponent mixtures.

We want to discuss these problems briefly and to state our approach to the modeling of FT slurry reactors.

As is known, the list of components participating in the FT synthesis comprises 50–100 individual chemical components, which exist in various thermodynamic states in the synthesis reactor and units, providing their subsequent treatment. Thus, CO, H_2, CO_2, CH_4, and C_2-C_3 are in the supercritical state, C_4-C_{10} hydrocarbons are in the state that is to a lesser or greater extent close to the critical state, and heavier fractions are in the liquid-only phase. In the general case, all components of the reaction mixture are present in both phases.

Despite this fact, the known mathematical models[23–25] consider only light gases (CO, H_2, CO_2, and CH_4) in the gas phase. The liquid phase is represented as a hydrocarbon "lump" which is determined component-wise by the Anderson–Shultz–Flory (ASF) distribution.[26] The reaction kinetic models consider the total rate of CO and H_2 conversion and the rate of the water–gas shift reaction.

It is obvious that these model conceptions do not adequately describe the actual process. A sufficient model must consider the complex composition of reaction mixtures and the complex reaction kinetics. Phase conversions must be calculated using rigorous thermodynamic models. In commercial slurry reactors,[27] chemical processes are accompanied by product separation by distillation. To obtain a better primary separation of heavy and light fractions, a condensate, obtained upon vapor gas cooling, is returned to the reactor. To design such a reactor and the best technology for the separation of products, the mathematical model must contain an extended kinetic model. The latter in combination with the thermodynamic models of phase split calculations will permit one to solve the problem set.

6.1. Kinetic Model of the Fischer–Tropsch Reaction. At present many research groups try to develop detailed kinetic models of FT reactions in the presence of various catalysts.[28–30] This is now possible because of extended potentialities for the experimental study of kinetics and the improvement of algorithms and calculation techniques required for mathematical processing of the experimental data.

Let us consider some methodical questions related to the development of the FT kinetic model using the experimental data of ref 31.

The experiment was performed in a slurry reactor over a finely dispersed alumina-supported cobalt catalyst promoted with zirconium. The catalyst properties, the procedures of preparation and activation, and the experimental data are reported elsewhere.[31]

To illustrate the method of the kinetic model development, we have chosen 16 isothermal (533 K) and isobaric (20 atm) runs from a series of extended tests,[31] in which the catalyst was treated with syngas flow for a long time with a view to obtain its steady-state activity.

The space velocity of the syngas flow at the reactor inlet (under normal conditions) was 1, 1.5, and 2 nL/g_{cat}/h, the inlet ratio of H_2/CO being 0.49, 0.75, and 1.0.

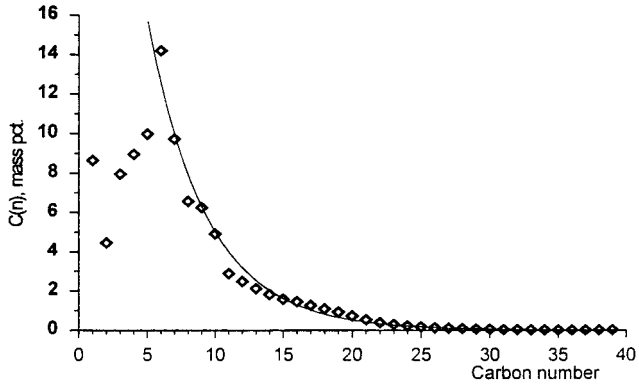

Figure 12. Hydrocarbons (alkanes + alkenes) mass percent vs the carbon number in the molecule. The line shows the ASF predicted distribution.

Table 8. Atomic Balance before and after Adjustment

atom	experiment inlet, g atom/h	experiment outlet, g atom/h	adjusted outlet, g atom/h	relative error, %
C	3.3868	3.6739	3.3868	7.81
O	3.3868	3.2816	3.3868	−3.21
H	6.7736	6.3646	6.7736	−6.43

The experimental data provide information about the rate of formation of 120 individual hydrocarbons (C_1−C_{40}, linear and branched paraffin, and α-olefins). For the kinetic model, data on linear and branched saturated hydrocarbons were summarized.

6.1.1. Primary Analysis of Experimental Data. To accurately balance the chemical elements at the reactor inlet and outlet, it is necessary to adjust the experimental data. Data were adjusted by the known reconciliation procedure[32a,b] which permits one to evaluate the experiment quality. If balance errors exceed the accuracy of measurements, one cannot develop an extended kinetic model. In the experiments, the adjusted molar fluxes of the components differ from the experimental data by 3−8%, which is within the limits of experimental error. The balance of chemical elements before and after adjustment is illustrated in Table 8.

The experimental data can be modeled using ASF-determined distributions. A typical distribution curve for C_1−C_{40} yield (mass %) versus the number of carbon atoms in a molecule is shown in Figure 12.

The hydrocarbon yield is maximum at $n = 6$ (n is the number of carbon atoms in a molecule). Thereafter, as n grows, the yield of hydrocarbons decreases exponentially. Note that the ASF distribution predicted with the α coefficient, characterizing the hydrocarbon chain growth probability[26] is valid only at $n \geq 6$ (see Figure 12). The chain growth probability, α, is a parameter of the kinetic model and is determined by the known statistical methods for processing the experimental data. These are discussed below.

6.1.2. Determination of α as a Function of the Reaction Mixture Composition. Let the sum of rates of n-hexane and n-hexene formation be the first element in a sequence approximated by the ASF distribution. Denote this rate as R_n^0, where $n^0 = 6$. Hereafter, the rate is expressed in gmol/(kg_{cat} h). The rate of formation of every subsequent hydrocarbon with a number of carbon atoms, $n^0 + i$, is determined as

$$R_{n^0+i} = R_{n^o}\alpha^i \qquad i = 1, 2, ..., Q \tag{66}$$

where $Q = N - n^0$, N is the greatest number of carbon atoms in a molecule, determined in the run ($N = 40$).

Summarizing series (66), we have

$$S_R = \sum_{i=0}^{Q} R_{n^0}\alpha^i = R_{n^0}(1 + S_\alpha) \tag{67}$$

where

$$S_\alpha = \sum_{i=1}^{Q} \alpha^i = \frac{\alpha(1 - \alpha^Q)}{1 - \alpha} \tag{68}$$

By normalizing the rates from eq 66 against sum S_{Rj}, one obtains dimensionless rates r_{n^0+i}:

$$r_{n^0+i} \equiv \frac{R_{n^0+i}}{S_R} = \frac{R_{n^0}\alpha^i}{S_R} = \alpha^i \frac{1 - \alpha}{1 - \alpha^{Q+1}} \qquad i = 0, 1, 2, ..., Q \tag{69}$$

Estimates for α were determined from each run by minimization of the objective function as

$$\psi(\alpha) = \sum_{i=0}^{Q}\{\ln \tilde{r}_{n^0+1} - [i \ln \alpha + \ln(1 - \alpha) - \ln(1 - \alpha^{Q+1})]\}^2 \rightarrow \min \tag{70}$$

where $\tilde{r}_{n^0+i}$ represents the experimental values of r_{n^0+i}.

Equation 70 was solved using the Gauss−Markwardt method.[32] The average relative residuals were 18−20%.

Usually, α is considered (except works in refs 28 and 29) as a constant value, which does not depend on the reaction mixture composition. But in the experiments discussed here, α depends on the current concentration of CO and H_2. Values of α increase with the carbon dioxide concentration and decrease with increasing hydrogen concentration.

To develop an explicit dependence of α on the concentrations of CO and H_2, we have tested several different equations, including those obtained by the reaction mechanism analysis.[28] On the basis of the statistics, the most reliable result was obtained for the following empirical equations:

$$\hat{\alpha} = A\frac{y_{CO}}{y_{CO} + y_{H_2}} + B \tag{71}$$

The estimated constants A and B are 0.2332 ± 0.0740 and 0.6330 ± 0.0420, respectively.

6.1.3. Chemical Reactions Used as a Basis for the Kinetic Model. The kinetic model of the FT process uses the following stoichiometric equations for the formation of individual hydrocarbons (methane, olefins, and paraffins):

$$CO + 3H_2 \rightleftarrows CH_4 + H_2O \tag{72}$$

$$CO + 2H_2 \rightarrow \frac{1}{n}C_nH_{2n} + H_2O \tag{73}$$

$$CO + \frac{2n + 1}{n}H_2 \rightarrow \frac{1}{n}C_nH_{2n+2} + H_2O \tag{74}$$

where $n = 2$−40 is the number of carbon atoms in a molecule.

The reaction mixture also contains carbon dioxide formed by the following reaction:

$$CO + H_2O \rightleftarrows CO_2 + H_2 \qquad (75)$$

The set of reactions (72)−(75) was used to describe the rates of individual component formation at $n \leq 6$. To describe the rate of saturated hydrocarbon formation for $n > 6$, we used eq 66 with allowance for the dependence between α and the reaction mixture composition from eq 71. Note that the amount of unsaturated hydrocarbons with $n > 6$ was rather small in the runs.

The reaction set (72)−(75) is simplified because paraffin hydrocarbons may result from both consecutive and parallel reactions. For instance, olefins may be primary products which are then hydrogenated to form saturated hydrocarbons.[33] A hydrocarbon chain may also grow because of the insertion of new molecules of CO and H_2 into the molecule. Nevertheless, on the basis of the experimental data from Lox et al.,[28,29] we concluded that each individual hydrocarbon could be considered as a primary reaction product.

6.1.4. Mathematical Model of the Kinetic Experiment. The general mathematical model of the isothermal isobar steady-state kinetic experiment,[30] performed in a perfectly mixed flow reactor, can be presented as a system of nonlinear algebraic equations written in vector terms:

$$\mathbf{M}^0 - \mathbf{M} + (g_{cat})\mathbf{Z}^T\mathbf{R}(\mathbf{y},\alpha(\mathbf{y}),\mathbf{K}) = \mathbf{0} \qquad (76)$$

where $\mathbf{M}^0 = [m_1^0, m_2^0, ..., m_{N_k}^0]^T$ is the N_k-dimensional vector of component molar fluxes (mol/h) at the reactor inlet, $\mathbf{M} = [m_1, m_2, ..., m_{N_k}]^T$ is the same vector at the reactor outlet, $\mathbf{Z}$ is a stoichiometric matrix of $N_r \times N_k$ dimension, $\mathbf{R} = [R_1, R_2, ..., R_{N_r}]^T$ is the N_r -dimensional vector of reaction rates, $\mathbf{y} = [y_1, y_2, ..., y_{N_g}]^T$ is the N_k-dimensional vector of the molar fractions of components in the vapor-gas phase, $\mathbf{K} = [K_1, K_2, ..., K_{N_p}]^T$ is the N_p-dimensional vector of kinetic constants, N_k is the number of components, N_r is the number of reactions, N_p is the number of kinetic constants (here, $N_p = N_r$), and g_{cat} is the catalyst sample (kg). The composition of the liquid phase, $\mathbf{x} = [x_1, x_2, ..., x_N]^T$, is determined on the basis of the assumption of a thermodynamic equilibrium between phases:

$$\mathbf{x} = \mathbf{K}^{eq}\mathbf{y} \qquad (77)$$

where $\mathbf{K}^{eq}$ is the $N_k \times N_k$ diagonal matrix of distribution constants determined by thermodynamic calculations.

The kinetic model identification problem is formulated by minimizing the error norm function,

$$Q = \sum_{i=1}^{N_{exp}} (\tilde{\mathbf{M}}_i - \hat{\mathbf{M}}_i)^T \mathbf{V}^{-1}{}_i (\tilde{\mathbf{M}}_i - \hat{\mathbf{M}}_i) \rightarrow \min \qquad (78)$$

subject to the constraints

$$\begin{aligned}
\mathbf{M}_1^0 - \hat{\mathbf{M}}_1 + (g_{cat})\mathbf{Z}^T\mathbf{R}(\hat{\mathbf{y}}_1,\alpha(\hat{\mathbf{y}}_1),\mathbf{K}) &= \mathbf{0} \\
\mathbf{M}_2^0 - \hat{\mathbf{M}}_2 + (g_{cat})\mathbf{Z}^T\mathbf{R}(\hat{\mathbf{y}}_2,\alpha(\hat{\mathbf{y}}_2),\mathbf{K}) &= \mathbf{0} \\
&\vdots \\
\mathbf{M}_{N_{exp}}^0 - \hat{\mathbf{M}}_{N_{exp}} + (g_{cat})\mathbf{Z}^T\mathbf{R}(\hat{\mathbf{y}}_{N_{exp}},\alpha(\hat{\mathbf{y}}_{N_{exp}}),\mathbf{K}) &= \mathbf{0}
\end{aligned} \qquad (79)$$

Here, N_{exp} is the number of experiments and $\mathbf{V}_i$ ($i = 1, 2, ..., N_{exp}$) is the $N_{exp} \times N_{exp}$ diagonal matrix of dispersions of the ith run. The signs "$\sim$" and "$\wedge$" denote the experimental and adjusted variables, respectively. For this problem of the model identification, both the kinetic constants involved in eq 80 and adjusted variables $\hat{\mathbf{M}}_i(\hat{\mathbf{y}})$ minimizing functional (78) are sought. In terms of the mathematical statistics, the obtained result meets the principle of maximum likelihood.[34] The problem is solved by the extended Marquardt-type procedure described elsewhere.[4,5]

6.1.5. Selection of the Rate Equations. To describe reaction rates, one sets an explicit form of the $\mathbf{R}$ vector components, that is, functions $R_j = R_j(\mathbf{y},\mathbf{K}(T,P))$, $j = 1, 2, ..., N_r$. Note that R_j may be expressed by concentrations $\mathbf{x}$ in the liquid phase using the distribution constants (77).

The major part of the kinetic studies did not go beyond rate expressions of the empirical power law type rate for the rate of carbon monoxide. Some authors derived Langmuir−Hinshelwood rate equations. The review of the kinetic equations is given in refs 22 and 26.

In refs 28 and 29 a detailed kinetic model was derived. The rate expressions for the hydrocarbon-forming reactions are based on elementary reactions corresponding to the carbide mechanism. Usually, kinetic experiments are not sensitive enough to all parameters responsible for the detailed reaction mechanism. Therefore, the chosen kinetic functions contain phenomenological elements. The best agreement between the experimental data and the model as well as a nice "conditionality" of rate constants were taken as a criterion of choosing the suitable approximations for rate equations.

Analyses of different versions of explicit R_j functions have shown that statistically reliable estimations may be obtained only for expressions that are linear in constants. Studying the power functions as

$$R_j = K_j y_{CO}^q\, y_{H_2}^p \qquad (80)$$

and comparing the experimental data, we have established some general regularities. Thus, for components C_2−C_5, the rate of unsaturated hydrocarbon formation is best described by

$$R_j = K_j y_{CO} y_{H_2}^2 \qquad (81)$$

The rate of saturated hydrocarbon formation is described by

$$R_j = K_j y_{H_2}^2 \qquad (82)$$

Unsaturated hydrocarbons are almost unobserved in a C_2 fraction and are also insignificant in the C_6 fraction. For the latter case, a rather good approximation of data was obtained for a number of saturated and unsaturated hydrocarbons as eq 82.

We suggest describing the rates of methane formation and vapor shift by the mass action law with allowance for their reversibility:

$$R_{CH_4} = K_{CH_4}\left(y_{CO} y_{H_2}^3 - \frac{y_{CH_4} y_{H_2O}}{K_{CH_4}^{eq}}\right) \qquad (83)$$

Table 9. Results of Kinetic Model Identification

	reactions	rate equations	model parameters, mol/(g_{cat} h)
1	$CH + 3H_2 \leftrightarrow CH_4 + H_2O$	$R_1 = K_1(y_{CO}y_{H_2}^3 - (1/K_{CH_4}^{eq})y_{CH_4}y_{H_2O})$	76.246 ± 1.312
2	$CO + H_2O \leftrightarrow CO_2 + H_2$	$R_2 = K_2\,(y_{CO}y_{H_2O}) - (1/K_{CO_2}^{eq})y_{CO_2}y_{H_2})$	5.653 ± 1.477
3	$CO + (5/2)H_2 \rightarrow (1/2)C_2H_6 + H_2O$	$R_3 = K_3y_{H_2}^2$	4.514 ± 0.746
4	$CO + (7/3)H_2 \rightarrow (1/3)C_3H_8 + H_2O$	$R_4 = K_4y_{H_2}^2$	6.344 ± 1.489
5	$CO + (9/4)H_2 \rightarrow (1/4C_4H_{10} + H_2O$	$R_5 = K_5y_{H_2}^2$	6.949 ± 1.168
6	$CO + (11/5)H_2 \rightarrow (1/5)C_5H_{12} + H_2O$	$R_6 = K_6y_{H_2}^2$	7.520 ± 0.826
7	$CO + (13/6)H_2 \rightarrow (1/6)C_6H_{14} + H_2O$	$R_7 = K_7y_{CO}y_{H_2}^2$	49.203 ± 0.612
8	$CO + 2H_2 \rightarrow (1/3)C_3H_6 + H_2O$	$R_8 = K_8y_{CO}y_{H_2}^2$	5.978 ± 1.728
9	$CO + 2H_2 \rightarrow (1/4)C_4H_8 + H_2O$	$R_9 = K_9y_{CO}y_{H_2}^2$	9.153 ± 0.823
10	$CO + 2H_2 \rightarrow (1/5)C_5H_{10} + H_2O$	$R_{10} = K_{10}y_{CO}y_{H_2}^2$	7.85 ± 1.249
11	$CO + (1 + y/2x)H_2 \rightarrow (1/x)C_xH_y + H_2O$	$R_{11} = R_7\alpha(1 - \alpha^N)/(1 - \alpha)$	

$$R_{CO_2} = K_{CO_2}\left(y_{CO}y_{H_2O} - \frac{y_{CO_2}y_{H_2}}{K^{eq}_{CO_2}}\right) \qquad (84)$$

The equilibrium constants are respectively $K^{eq}_{CH_4} = 2 \times 10^{10}$ and $K^{eq}_{CO_2} = 74.1474$ at 533 K and 2.0 MPa.

To efficiently solve a minimization problem, (78)−(79), it is necessary to choose good initial approximations of the constants and variance error matrix. These values were found for every individual hydrocarbon, C_1−C_6, by the least-squares technique when the functions set by eqs 81 and 82 were studied at once.[30] Relative residuals, obtained upon such primary processing of data, were used later for the estimation of **V** matrix elements.

To reduce the problem dimensionality, we used eq 66 with an allowance for eq 71, which nicely described the carbon series starting from C_7. Because of this arrangement, in each run one can group all individual hydrocarbons starting from C_7, as an averaged component C_xH_y, where x and y are the numbers of atoms of carbon and hydrogen and index i indicates the experimental number. Values of x and y were found by

$$x_i = \frac{\sum_{j=n^0+1}^{N} j\alpha^{j-n^0}}{\sum_{j=n^0+1}^{N} \alpha^{j-n^0}}; \qquad y_i = 2x_i + 2, \quad i = 1, 2, ..., N_{exp} \qquad (85)$$

$\hat{\alpha}$ was found for each run by eq 71. Thus, the dimensionality of problem (81)−(84) was reduced to 14, and vector **M** was formed from molar fluxes of the following components: CO, H_2, CO_2, H_2O, CH_4, C_2H_6, C_3H_6, C_3H_8, C_4H_8, C_4H_{10}, C_5H_{10}, C_5H_{12}, C_6H_{14}, and C_xH_y. The formation of the group component may be written as

$$CO + \frac{y_i + 2x_i}{2x_i}H_2 \rightarrow \frac{1}{x_i}C_{x_i}H_{y_i} + H_2O \qquad (86)$$

The rate of this reaction in the kinetic model is set by the equation as

$$R_{C_xH_y} = R_{C_6}\sum\alpha^{j-6} \qquad (87)$$

where R_{C_6} is the total rate of hexane and hexene formation.

6.1.6. Results of the Kinetic Model Identification. The statistics obtained by identification of the kinetic model is as follows:

(1) Number of degrees of freedom, 228

(2) Value of t criterion at the 95% confidence level, 1.966

(3)Root-mean-square absolute deviation of experimental and calculated values of molar fluxes (gmol/h), 0.052 11

(4) Root-mean-square relative deviation of experimental and calculated molar fluxes (%), 17.29

(5) Root-mean-square disbalance of eq 80 (gmol/h), 0.000 028 85

The parameter estimates are given in Table 9. Figure 13a−d shows a comparison between the experimental and the calculated outlet mole flows of the components.

As shown by statistical summary, providing an average relative error of 17%, the model fits the experimental data well and may be used for mathematical modeling of the reactor.

6.2. Mathematical Model of the Reactor Unit. A scheme of the reactor unit as an element of the whole process scheme is shown in Figure 14.

Syngas (FLO_G) with a set ratio of CO/H_2 is directed to the reactor (unit B_1). Condensate (FL0_L) is also directed to B_1 after separation of water in B_3 (separator). T_1 and P_1 are the working parameters of the reactor. The liquid (FL1_L) and vapor-gas (FL1_G) reaction products leave the reactor. The latter goes to a cooler (unit B_2). Here, at T_2 and P_2 (temperature and pressure of the cooler), a part of the high-boiling synthesis products is condensed. Vapor-gas FL2_G, containing a part of unreacted CO and H_2 and light products of synthesis, is directed for further processing. The liquid condensate (FL2_L) is fed into the separator (unit B_3), where it is divided into two liquid phases, such as a water phase (FL3_L_3) and hydrocarbon phase (FL3-L_1) at T_3 and P_3 (temperature and pressure in the separator). In this case, a new vapor-gas phase (FL3_G) may form. The hydrocarbon fraction (FL3_L_1) is divided into two fluxes: FLO_L is returned to the reactor, and FL4_L is directed for further processing. The ratio between the fluxes FL0_L and FL3_L_1 is set by coefficient β. Coefficient β, T_2, P_2, T_3, and P_3 are the controlling process parameters. The fluxes dimensionally are kmol/h.

6.2.1. Main Prerequisites of the Model. Reflux is meant to provide the steady-state operation of the reactor. At 530−550 K and under reaction conditions, the dry syngas fed into the reactor is permanently saturated with hydrocarbon vapors, which are released together with the gas reaction products. As a result, the liquid volume may gradually decrease in the reactor.

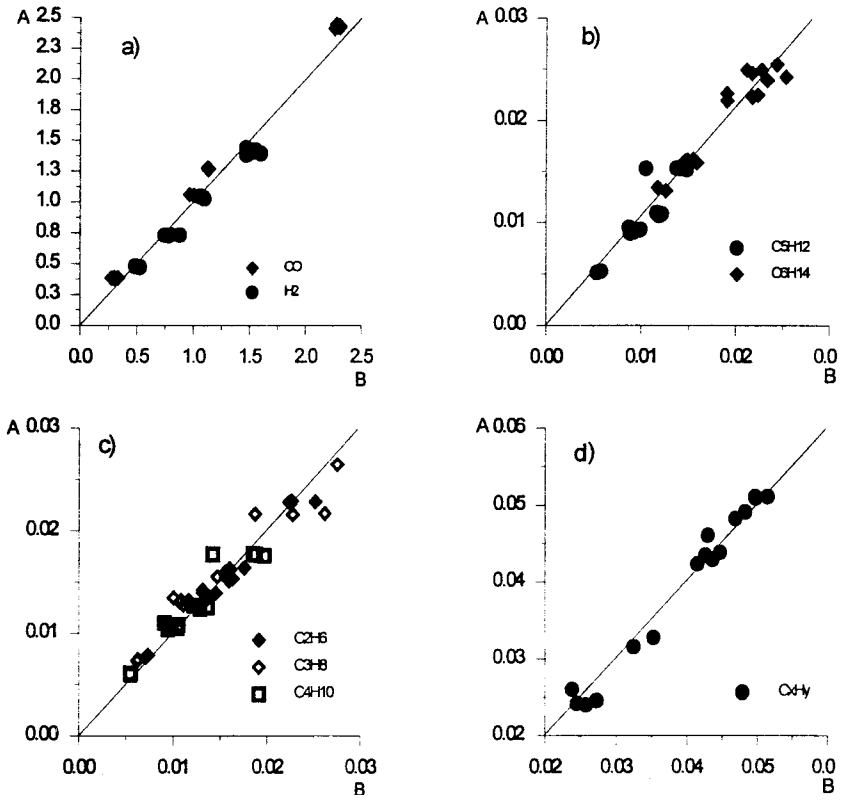

Figure 13. Comparison between experimental (B) and calculated (A) molar fluxes (mol/h) of CO and H_2 (a), C_5H_{12} and C_6H_{14} (b), C_2H_6, C_3H_8, and C_4H_{10} (c), and C_xH_y (d) at the reactor outlet.

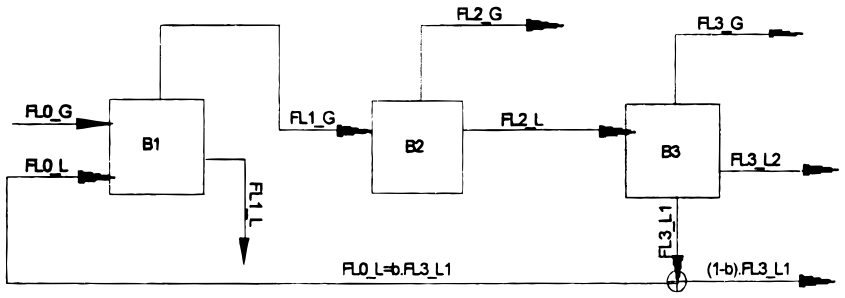

Figure 14. Scheme of reactor unit.

So the steady-state process regime is not provided. Reflux compensates removal of the liquid phase from the reactor and provides the steady-state flow of the liquid phase in the reactor. In the limiting case, this flow may be zero, but negative values are not permitted.

It is expected that phases are completely mixed in the reactor (isothermal and isobar regimes). Changes in the overall molar flow of components are caused by chemical reactions proceeding in the reactor. Phase distribution of components and yields of each phase are determined by equilibrium phase transitions.

The list of components comprises 35 individual substances ($N_k = 35$) as CO, H_2, CO_2, H_2O, CH_4, C_3-C_5 olefins, and C_2-C_{28} *n*-paraffins.

The mathematical description of the above process scheme with allowance for the prerequisites discussed is stated below.

(a) Reactor. Inlet fluxes are set $m_{i,G}^{(0)}$ and $m_{i,L}^{(0)}$ ($m_{iL}^{(0)} = \beta m_{iL}^{(3)}$):

$$m_i^{(0)} = m_{i,L}^{(0)} + m_{i,G}^{(0)} \tag{88}$$

$$m_{1G}^{(0)} = m_{CO}^{(0)}; \qquad m_{2G}^{(0)} = m_{H_2}^{(0)}; \qquad m_{iG}^{(0)} = 0; \quad i = 3, 4, ..., N_k \tag{89}$$

$$\mathrm{FL0\_G} = m_{CO}^{0} + m_{H_2}^{0}; \qquad \mathrm{FL0\_L} = \sum_{i=1}^{N_k} m_{iL}^{0} \tag{90}$$

The design of reactors is reduced to solution of the following algebraic equations regarding the unknowns $m_i^{(1)}$, $m_{iL}^{(1)}$, and $m_{iG}^{(1)}$:

$$m_i^0 - m_i^{(1)} + q_i(\mathbf{y}^{(1)}, T_1, P_1) = 0 \tag{91}$$

$$q_i = g_{cat} \sum_{j=1}^{N_r} Z_{ji} R_j(\mathbf{y}^{(1)}, T_1, P_1) \tag{92}$$

$$\mu_i^{G}(T_1, P_1, \mathbf{y}^{(1)}) - \mu_i^{L}(T_1, P_1, \mathbf{x}^{(1)}) = 0 \tag{93}$$

and with allowance for balance relations and other obvious restrictions:

$$m_i^{(1)} = m_{i,\mathrm{L}}^{(1)} + m_{i,\mathrm{G}}^{(1)} \quad (94)$$

$$\mathrm{FL1\_L} = \sum_{i=1}^{N} m_{i\mathrm{L}}^{(1)}; \qquad \mathrm{FL1\_G} = \sum_{i=1}^{N} m_{i\mathrm{G}}^{(1)} \quad (95)$$

$$x_i^{(1)} = \frac{m_{i\mathrm{L}}^{(1)}}{\mathrm{FL1\_L}}; \qquad y_i^{(1)} = \frac{m_{i\mathrm{G}}^{(1)}}{\mathrm{FL1\_G}} \quad (96)$$

$$\sum x_i^{(1)} = 1 \sum y_i^{(1)} = 1 \quad (97)$$

$$i = 1, 2, ..., N_k$$

(b) Cooler. To solve the problem of flux FL1_G (fed into the cooler) division into two equilibrium fluxes FL2_G (vapor-gas) and FL_2L (liquid), we use the model (20)−(26) at T_2 and P_2. The overall composition is set as $z_i = y_i^{(1)} z_1 = y^{(1)}$, where $i = 1, 2, ..., N_k$. As a result of the solution, one obtains phase concentrations $x_i^{(2)}$ and $y_i^{(2)}$ as well as phase fractions $W_{\mathrm{L}}^{(2)}$ and $W_{\mathrm{G}}^{(2)}$ ($W_{\mathrm{L}}^{(2)} + W_{\mathrm{G}}^{(2)} = 1$), which determine molar fluxes of components in two phases after the cooler

$$m_{i\mathrm{G}}^{(2)} = W_{\mathrm{G}}^{(2)}\, m_{i\mathrm{G}}^{(1)}; \qquad m_{i\mathrm{L}}^{(2)} = (1 - W_{\mathrm{G}}^{(2)}) m_{i\mathrm{G}}^{(1)} \quad (98)$$

$$\mathrm{FL2\_G} = \sum m_{i\mathrm{G}}^{(2)}; \qquad \mathrm{FL2\_L} = \sum m_{i\mathrm{L}}^{(2)} \quad (99)$$

$$i = 1, 2, ..., N_k$$

(c) Separator. FL2_L is directed to the separator. This flux may contain large amounts of water. At T_3 and P_3 in the separator, flux FL2_L is divided concurrently into two liquid phases (liquid and hydrocarbon), and an outflow as vapor-gas. The incoming flux is thus divided into three equilibrium phases in the separator. This separation follows a model similar to that of (20)−(26), and the systems equilibrium equations and material balance equations are solved simultaneously:

$$\mu_{i\mathrm{L}_1}^{(3)}(T_3, P_3, \mathbf{x}_{\mathrm{L}_1}^{(3)}) - \mu_{i\mathrm{G}_1}^{(3)}(T_3, P_3, \mathbf{y}^{(3)}) = 0 \quad (100)$$

$$\mu_{i\mathrm{L}_2}^{(3)}(T_3, P_3, \mathbf{x}_{\mathrm{L}_2}^{(3)}) - \mu_{i\mathrm{G}_1}^{(3)}(T_3, P_3, \mathbf{y}^{(3)}) = 0 \quad (101)$$

$$z_i \equiv x_{i\mathrm{L}}^{(2)} = W_{\mathrm{G}}^{(3)} y_i^{(3)} + W_{\mathrm{L}_1}^{(3)} x_{i\mathrm{L}_1}^{(3)} + W_{\mathrm{L}_2}^{(3)} x_{i\mathrm{L}_2}^{(3)} \quad (102)$$

$$\mathrm{FL3\_G} = W_{\mathrm{G}}^{(3)} \mathrm{FL2\_L}; \qquad m_{i\mathrm{G}}^{(3)} = \mathrm{FL3\_G} \times y^{(3)} \quad (103)$$

$$\mathrm{FL3\_L_1} = W_{\mathrm{L}_1}^{(3)} \mathrm{FL2\_L}; \qquad m_{i\mathrm{L}_1}^{(3)} = \mathrm{FL3\_L_1} \times x_{i\mathrm{L}_1}^{(3)} \quad (104)$$

$$\mathrm{FL3\_L_2} = W_{\mathrm{L}_2}^{(3)} \mathrm{FL2\_L}; \qquad m_{i\mathrm{L}_2}^{(3)} = \mathrm{FL3\_L2} \times x_{i\mathrm{L}_2}^{(3)} \quad (105)$$

$$W_{\mathrm{G}}^{(3)} + W_{\mathrm{L}_1}^{(3)} + W_{\mathrm{L}_2}^{(3)} = 1 \quad (106)$$

$$\sum y_i^{(3)} = 1; \qquad \sum x_{i\mathrm{L}_1}^{(3)} = 1; \qquad \sum x_{i\mathrm{L}_2}^{(3)} = 1 \quad (107)$$

(d) Reflux. Hydrocarbon phase $\mathrm{FL3\_L_1}$ is divided into flux $\mathrm{FL0\_L} = \beta \times \mathrm{FL3\_L_1}$, which is returned to the reactor, and $(1-\beta) \times \mathrm{FL3\_L_1}$, which is further processed as a semiproduct. β is the process-controlling parameter.

6.2.2. Algorithm for Process Scheme Calculation. Because the scheme (Figure 15) contains a closed cycle with respect to liquid flow, the steady-state solution for the whole scheme is obtained by the successive iteration method. An arbitrary value of FL0_L and its composition are set as an initial approximation, and then the problems for the reactor, cooler, and separator are solved in succession. As a first approximation of FL3_L is obtained (at given β), the following approximation of FL0_L is determined. Iterations are continued until steady-state values of all fluxes in the technological process scheme are determined.

Iteration convergence to the steady-state solution is determined by the existence of problem solution in the reactor at the given pressure and temperature, which depend primarily on β.

Let $m_i^{(1)}$ be the current approximation for the total molar flux of the ith component at the reactor outlet. Molar fractions (overall composition) are determined as $z_i = m_i^{(1)}/\sum m_i^{(1)}$. At the given overall composition, one solves system (20)−(26) with a view to divide this mixture into equilibrium phases and find equilibrium concentrations and phase yields.

Consider conditions for such solution existence. Function φ (eq 25), determining a phase fraction, is a continuously decreasing function of W_x. The solution exists at $0 \le W_x \le 1$ if the following two inequalities are fulfilled:

$$\sum_{i=1}^{N_k} z_i K_i \ge 1 \quad (108)$$

$$\sum_{i=1}^{N_k} z_i / K_i \ge 1 \quad (109)$$

The flux FL1_L is

$$\mathrm{FL1\_L} = W_x \sum_{i=1}^{N_k} m_i^{(1)} \quad (110)$$

If (108) is not fulfilled, we have a nonphysical solution $W_x < 0$; that is, FL1_L is a negative flux. This means that a mixture of **z** composition (at a chosen value of β and given T_1 and P_1 in the reactor) is an unsaturated vapor gas, which does not condense under these conditions. To ensure its equilibrium saturation, components must go from the liquid into the gas. To put it differently, the reactor operates under a regime of liquid-phase evaporation, resulting in a progressive decrease of liquid in the reactor.

Theoretically, the problem may have no solution if inequality (109) is not fulfilled. In this case, we have either a nonphysical solution, $W_x > 1$, or a probable complete condensation of mixture in the reactor. Because the mixture contains supercritical components (unreacted CO, H_2, or formed CH_4, CO_2, etc.), this critical case is not realized. Moreover, one may obtain a nonphysical solution with respect to $W_x < 1$. Such a situation is usually observed when FL0_L is not formed or its amount is insufficient. As was noted, the composition and amount of flux FL0_L are regulated by such process parameters as β, T_2, P_2, T_3, and P_3. If β is properly chosen, the steady-state regime over the whole system is established during 5−10 iterations.

6.2.3. Calculation Results. In this work we do not intend to optimize the scheme, and the selected calculation results are primarily used to illustrate how reflux provides a steady-state operation regime in the reactor. In the examples, β and the temperature of the cooler are varied. The temperature in the separator was set

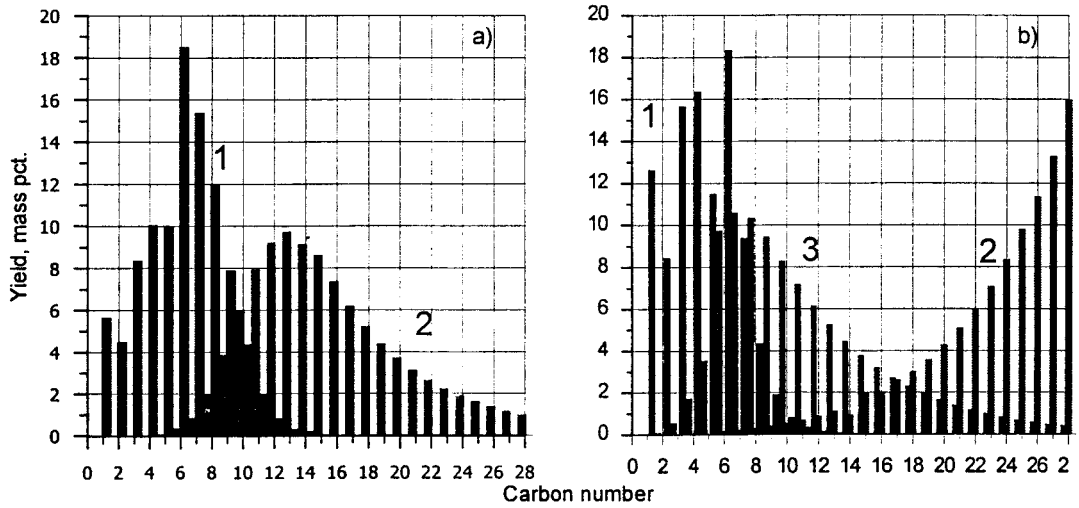

Figure 15. (a, b) Distribution of hydrocarbons in the product fluxes released from the reactor unit. The temperature of the cooler is 373 K. (a) $\beta = 1$, (b) $\beta = 0.5$. (1) vapor-gas flow after the cooler, (2) liquid flow after the reactor, and (3) liquid flow after the separator.

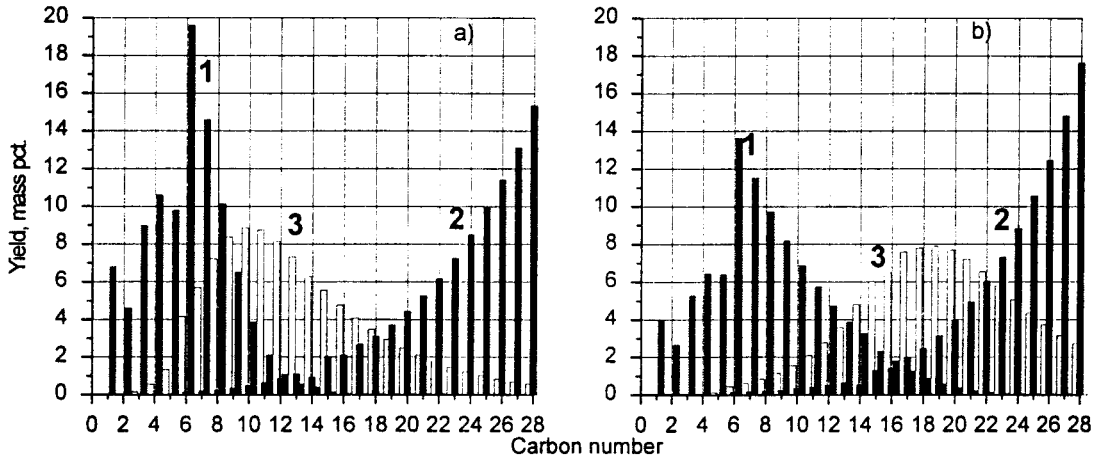

Figure 16. (a, b) Distribution of hydrocarbons in the product fluxes released from the reactor unit. $\beta = 0.5$. The temperature of the cooler is (a) 423 K, (b) 473 K. (1) vapor-gas flow after the cooler, (2) liquid flow after the reactor, and (3) liquid flow after the separator.

equal to that of the cooler, and the pressure in the whole system was 20 atm. Space velocity (0.68 $nm^3/kg_{cat}/h$) and a ratio between CO and H_2 (1:1) in the initial gas were kept constant.

Figure 16a,b shows graphs of the hydrocarbon distribution in fluxes of FL1_L (liquid hydrocarbons after the reactor), FL3_L1 (liquid hydrocarbons after the separator), and FL2_G (hydrocarbons in the vapor gas after the cooler) at $\beta = 1$ (Figure 16a) and $\beta = 0.5$ (Figure 16b), respectively. The pressure in the system is 20 atm, and the temperature of the cooler is 373 K.

At $\beta = 1$, FL1_L and FL2_G fluxes of semiproducts are released from the reactor. At $1 > \beta > 0$, $(1 - \beta)$-FL3_L1 is also observed among the product fluxes.

At $\beta = 1$, the graphs of the light and middle fractions are easily distinguished. The light fraction consists of hydrocarbons of FL2_G and the middle fraction consists of hydrocarbons of flux FL1_L. At $\beta = 0.5$, three fractions of semiproducts that are distinctly divided into light, middle, and heavy hydrocarbons are chosen. Here, the light fraction consists of hydrocarbons of flux $(1 - \beta)$FL3_1, and the heavy fraction consists of hydrocarbons of flux FL1_L.

In Figure 16a,b, similar distributions are given for $\beta = 0.5$, the temperature of the cooler being 423 K (17a) and 473 K (17b). The figure shows that, at the given β, the composition and the fraction yield can be controlled by cooler temperature. As the temperature in the cooler rises, separation is more pronounced.

In conclusion, we want to emphasize that reflux is required for steady-state operation of the slurry reactor upon FT synthesis. Note that laboratory systems intended to study the kinetics of the FT synthesis are usually supplied with a "reverse cooler" ($\beta = 1$).[35,36] In the prototypes of the FT liquid-phase reactors,[37,38] some portions of liquid feedstock were also returned in the process. The commercial slurry reactor (SSPD, Sasol slurry phase distillate reactor) works on the same principle at the SASOL-II plant.[27]

Corresponding equations for the enthalpy balance are supplied to the model for the technological calculations. Enthalpies are calculated at stationary values of fluxes and concentrations. As a result, heat fluxes, providing isothermal regimes in each device, are determined.

7. Conclusion

A line from the poem by Aris R., "Do all that you know and try all that you don't," [39] stimulated the performance of this work. We emphasize the leading role of thermodynamic calculations in the modeling of multiphase processes and reactors. Because the division of fluxes into equilibrium phases in a reactor unit requires knowledge of the composition of every reaction mixture

component, it is necessary to have an expanded kinetic model of the reaction, which helps to predict the detailed composition of reaction products. Though mathematical models of reactors incorporating the kinetics, thermodynamics, and multicomponent structure of the reaction mixture are rather cumbersome, they help to understand the process essence, and thus to develop the optimal technology.

We do not claim that our models are complete or that our solution algorithms are necessarily optimal. In our minds, the doors are open for further investigations.

Acknowledgment

The authors would like to thank Dr. Jeffrey A. Manion from the National Institute of Standards and Technology, Gaithersburg, MD for useful comments regarding this manuscript.

Literature Cited

(1) Reid, R. C.; Prausnitz, J. M.; Sherwood, T. K. *The Properties of Gases and Liquids;* McGraw-Hill: New York, 1977.

(2) Soave, G. Equilibrium Constants from a Modified R.K. Equation of State. *Chem. Eng. Sci.* **1972**, *27*, 1197.

(3) Kogan, V. B.; Fridman, V. M.; Kafarov, V. V. *An Equilibrium between Liquid and Vapor*; Izd-vo Nauka: Moscow-Leningrad, 1966 (in Russian); Vol. 2.

(4) Valko, P.; Vajda, S. An Extended Marquardt-Type Procedure for Fitting Error-in-Variables Models. *Comput. Chem. Eng.* **1987**, *11*, 37.

(5) Yermakova, A.; Gudkov, A. V.; Anikeev, V. I. Identification of Kinetic Models. *Kinet. Katal.* **1997**, *38*, 309.

(6) Krichevskii, I. R. Phase Equilibria in Solutions at High Pressures. Goskhimizdat: Moscow-Leningrad, 1952.

(7) Anderson, T. F.; Prausnitz, J. M. Computational Methods for High-Pressure Phase Equilibria and Other Fluid Phase Properties Using a Partition Function. 2. Mixtures. *Ind. Eng. Chem. Process Des. Dev.* **1980**, *19*, 9.

(8) Michelsen, M. L. The Isothermal Flash Problem. Part II. Phase Split Calculation. *Fluid Phase Equilibr.* **1982**, *9*, 21.

(9) *Thermodynamics of Liquid−Vapor Equilibrium*; Morachevskii, A. G., Ed.: Khimiya: Leningrad, 1989.

(10) Sun, A. C.; Seider, W. D. Homotopy−Continuation Method for Stability Analysis in the Global Minimization of the Gibbs Free Energy. *Fluid Phase Equilibr.* **1995**, *103*, 213.

(11) Cairns, B. P.; Furzer, I. A. Multicomponent Three-Phase Azeotropic Distillation. 2. Phase-Stability and Phase-Splitting Algorithms. *Ind. Eng. Chem. Res.* **1990**, *29*, 1364.

(12) Allgower, E.; Georg, K. Simplical and Continuation Methods for Approximating Fixed Points and Solutions to Systems of Equations. *SIAM Rev.* **1980**, *22*, 28.

(13) Choi, S. H.; Harney, D. A.; Book, N. L. A Robust Path Tracking Algorithm for Homotopy Continuation. *Comput. Chem. Eng.* **1996**, *20*, 647.

(14) Gurevich, G. R.; Brusilovkii, A. I. A Handbook for Calculations of Phase States and Properties of Gas-Condensate Mixtures, Nedra: Moscow, 1984.

(15) Peng, D. Y.; Robinson, D. B. A Rigorous Method for Predicting the Critical Properties of Multicomponent System from an Equation of State. *AIChE J.* **1977**, *23*, 137.

(16) Heidemann, R. A.; Khalil, A. M. The Calculation of Critical Points. *AIChE J.* **1980**, *26*, 769.

(17) Karapetynts, M. Kh. *Chemical Thermodynamics*; Khimiya: Moscow, 1975.

(18) Savage, E. P.; Gopalan, S.; Mizan, T. I.; Martino, Ch. J.; Brock, E. E. Reactions at Supercritical Conditions: Applications and Fundamentals. *AIChE J.* **1995**, *41*, 1723.

(19) Lang, X.; Akgerman, A.; Bukur, D. B. Steady-State Fischer−Tropsch Synthesis in Supercritical Propane. *Ind. Eng. Chem. Res.* **1995**, *34*, 72.

(20) Yokota, K.; Fujimoto, K. Supercritical-Phase Fischer−Tropsch Synthesis Reaction. 2. The Effective Diffusion of Reactant and Products in the Supercritical-Phase Reaction. *Ind. Eng. Chem. Res.* **1991**, *30*, 95.

(21) Fiquiere, P.; Hom, J. F.; Laugier, S.; Renon, H.; Richon, D.; Szwarc, H. Vapor-Liquid Equilibrium Up to 40000 KPa and 400 °C: A New Static Method. *AIChE J.* **1980**, *26*, 872.

(22) Saxena, S. C. Bubble Column Reactors and Fischer−Tropsch Synthesis. *Catal. Rev.-Sci. Eng.* **1995**, *37*, 227.

(23) Deckwer, W.-D.; Serpemen, Y.; Ralek, M.; Schmidt, B. Fischer−Tropsch Synthesis in the Slurry Phase on Mn/Fe Catalysts. *Ind. Eng. Chem. Process Des. Dev.* **1982**, *21*, 222.

(24) Deckwer, W.-D.; Serpemen, Y.; Ralek, M.; Schmidt, B. Modeling the Fischer−Tropsch Synthesis in the Slurry Phase. *Ind. Eng. Chem. Process Des. Dev.* **1982**, *21*, 231.

(25) Deckwer, W. D.; Serpemen, Y.; Ralek, M.; Schmidt, B. On the Relevance of Mass Transfer Limitations in the Fischer−Tropsch Slurry Process. *Chem. Eng. Sci.* **1981**, *36*, 765.

(26) Anderson, R. B. *Fischer−Tropsch Synthesis*; Academic Press: New York, 1984.

(27) Jager, B.; Espinoza, R. Advances in Low-Temperature Fischer−Tropsch Synthesis. *Catal. Today* **1995**, *23*, 17.

(28) Lox, E. S.; Froment, G. F. Kinetics of the Fischer−Tropsch Reaction on a Precipitated Promoted Iron Catalyst. 1. Experimental Procedure and Results. *Ind. Eng. Chem. Res.* **1993**, *32*, 61.

(29) Lox, E. S.; Froment, G. F. Kinetics of the Fischer−Tropsch Reaction on a Precipitated Promoted Iron Catalyst. 2. Kinetic Model. *Ind. Eng. Chem. Res.* **1993**, *32*, 71.

(30) Yermakova, A.; Anikeev, V. I.; Gudkov, A. V. A Macrokinetic Model of the Fischer−Tropsch Reaction on the Cobalt Containing Catalyst Suspended in Liquid Hydrocarbons. *Zh. Prikl. Khim.* **1997**, *70*, 1500 (in Russian).

(31) *Novel Fischer−Tropsch Slurry Catalysts and Process Concepts for Selective Transportation Fuel Production*; Report DOE/PC/70030-T7/DE87 06115/Contract No. DE-AC22−84PC70030; Department of Energy: Washington, DC.

(32) (a) Valko, P.; Vajda, S. *Advanced Scientific Computing in BASIC with Applications in Chemistry, Biology and Pharmacology*; Elsevier: Amsterdam, 1989. (b) Yermakova, A.; Anikeev, V. I.; Gudkov, A. V.; Bobrin, A. S. "Experimental Setup-PC" for Kinetic Study and Design of Kinetic Models for Complex Reactions. *Theor. Found. Chem. Eng.* **1995**, *1*, 61 (in Russian).

(33) Madon, R. J.; Taylor, W. F. Fischer−Tropsch Synthesis on a Precipitated Iron Catalyst. *J. Catal.* **1981**, *69*, 32.

(34) Reilly, P. M.; Patino-Leal, H.; Bayesian, A. Study of the Error-in-Variables Model. *Technometrics* **1981**, *23*, 221.

(35) Bukur, D. B.; Patel, S. A.; Xiaosu Lang. Fixed Bed and Slurry Reactor Studies of Fischer−Tropsch Synthesis on Precipitated Iron Catalyst. *Appl. Catal.* **1990**, *61*, 329.

(36) Ledakowicz, S.; Nettelhoff, H.; Kokuun, R.; Deckwer, W. D. Kinetics of the Fischer−Tropsch Synthesis in the Slurry Phase on a Potassium-Promoted Iron Catalyst. *Ind. Eng. Chem. Process Des. Dev.* **1985**, *24*, 1043.

(37) Storch, H.; Golambic, N.; Anderson, R. *The Fischer−Tropsch and Related Syntheses*; Wiley: New York, 1951.

(38) Yan, Yu. B.; Nefedov, B. K. *Synthesis on Carbon Oxides*; Khimiya: Moscow, 1987.

(39) Aris, R. *The Optimal Design of Chemical Reactors: A Study in Dynamic Programming*; Bellman, R., Ed.; Mathematics in Science and Engineering; Academic Press: New York, 1961; Vol. 3.

Received for review August 2, 1999
Revised manuscript received January 6, 2000
Accepted January 11, 2000

IE9905761